Copy No. 38

NASA Program Apollo Working Paper No. 1119

A STUDY OF THE EFFECT OF REDUCED LAUNCH VEHICLE ENGINE GIMBAL ANGLE LIMITS ON THE TIME AVAILABLE FOR APOLLO HARD-OVER-GIMBAL ABORT AT MAXIMUM DYNAMIC PRESSURE (U)

DISTRIBUTION AND REFERENCING

This paper is not suitable for general distribution or referencing. It may be referenced only in other working correspondence and documents by participating organizations.

NATIONAL AERONAUTICS AND SPACE ADMINISTRATION
MANNED SPACECRAFT CENTER
Houston, Texas

~~CONFIDENTIAL~~

NASA Program Apollo Working Paper No. 1119

A STUDY OF THE EFFECT OF REDUCED LAUNCH VEHICLE ENGINE GIMBAL ANGLE LIMITS ON THE TIME AVAILABLE FOR APOLLO HARD-OVER-GIMBAL ABORT AT MAXIMUM DYNAMIC PRESSURE (U)

Prepared by: William E. Thomas, Jr.
William E. Thomas, Jr.
ASTD, Flight Mechanics Branch

Authorized for Distribution:

Warren Gillespie, Jr.
for Maxime A. Faget
Assistant Director for Engineering and Development

NATIONAL AERONAUTICS AND SPACE ADMINISTRATION

MANNED SPACECRAFT CENTER

HOUSTON, TEXAS

~~CONFIDENTIAL~~

TABLE OF CONTENTS

LIST OF TABLES

LIST OF FIGURES

A STUDY OF THE EFFECT OF REDUCED LAUNCH VEHICLE ENGINE GIMBAL ANGLE LIMITS ON THE TIME AVAILABLE FOR APOLLO HARD-OVER-GIMBAL ABORT AT MAXIMUM DYNAMIC PRESSURE (U)

SUMMARY

A study has been made to determine the feasibility of increasing the time available for a hard-over-gimbal abort at maximum dynamic pressure by reducing the Saturn IB and Saturn V booster engine maximum allowable gimbal angles to those values required for the nominal Apollo missions. This study was made because of the extremely short time presently available for a booster-engine hard-over abort of the Apollo spacecraft at maximum q.

In the study, abort time, for a specific type of hardover failure, refers to the minimum time available from overrate sensing of a hard-over-gimbal abort situation to vehicle structural failure (structural failure was simulated by arbitrarily large structural loads). The study considers both single gimbal failures and oscillatory failures. Since this was a general feasibility study rather than a detailed analysis, the study was limited to rigid body motion and yaw plane winds.

The results of the study indicate that the maximum booster gimbal angles for the Saturn IB and Saturn V vehicles could possibly be reduced from 8° to 6.5°, and from 5.15° to 3°, respectively, without loss of adequate control for the specific Apollo missions considered. For a single gimbal failure, decreasing the Saturn IB angle to 6.5° results in no increase in abort time, and decreasing the Saturn V angle to 3° increases abort time by 0.18 second. For oscillatory failures, there is only a 0.04 second increase in abort time for the Saturn IB, but there is a 0.60 second increase in abort time for the Saturn V. With the exception of the Saturn V oscillatory case, the study results show no significant increases in available abort time at maximum q due to maximum gimbal angle reduction.

An analysis was also made of available abort time at booster burnout. The results indicated the desirability of further study in this region as soon as more accurate vehicle structural data becomes available.

INTRODUCTION

The control engines on the S-1A and S-1C boosters (figs. 1 and 2) are presently capable of maximum angular deflections of 8° and 5.15° (square pattern) respectively. These deflection limits are designed to meet the control requirements of numerous vehicle configurations and missions which have been considered to date. The time available for an abort of the Apollo spacecraft from the Saturn IB or Saturn V vehicle when a hardover engine failure occurs is, assuming rigid body motion, a function of the inverse of these maximum angles. Because of the small amount of time available for abort in the case of an engine hard-over failure at maximum dynamic pressure, a study has been made to determine the feasibility of increasing abort times by restricting gimbal excursions to those maximum angles which would be required for each of two typical Apollo-Saturn configuration-mission combinations.

The basic study considers simultaneous unidirectional single gimbal failure of all control engines, since this is the mode of hard-over-gimbal failure usually considered in mission analysis. From the standpoint of available abort time, the most extreme type of hard-over-gimbal failure is an oscillatory type of failure; that is, control engines hardover in one direction, followed shortly by hard-over motion in the opposite direction. Although this mode of failure is extremely unlikely, it is important to recognize and define a worst case; therefore, oscillatory failures have also been included. In this study, abort time for a specific abort mode mentioned above, refers to the minimum time available from the sensing of an abort situation by an overrate sensor until the vehicle fails structurally. Actual structural failure data could not be obtained for either of the vehicles considered; therefore, vehicle breakup was simulated by arbitrarily large structural loads.

The present study considers yaw plane failures only; that is, the atmospheric wind vector and engine deflections were assumed perpendicular to the trajectory plane. Headwinds and tailwinds in the pitch plane were not considered since the purpose of this study was not to give detailed analyses or to define gimbal angles, but to indicate the general feasibility of the reduced maximum gimbal angle concept by selecting a fairly reasonable reduced maximum gimbal angle and studying the resulting effect on abort time. Engine-out capability was not considered since it was not expected that this will be a requirement for the Apollo missions.

The analysis can be broken down into two basic phases. The first phase consisted of the determination of the maximum gimbal angles required for rigid body control, under nominal vehicle conditions, of the Saturn IB and Saturn V vehicles when flying through yaw plane winds

based on the nondirectional 95 percent probability-of-occurrence idealized wind speed profile envelope and the 99 percent probability wind shear spectrum envelopes for Cape Kennedy (ref. 1). The second phase consisted of hardover engine studies considering both the existing maximum gimbal angles and maximum gimbal angles based on the results of the first phase. The time available from the sensing of an overrate abort condition until the vehicle reached a preselected high structural loading (assumed structural failure) was then compared for the two different maximum gimbal angle cases.

A brief study was also made of abort at booster burnout using the reduced gimbal angles.

SYMBOLS

A	Vehicle axial acceleration, g units
C_{N_α}	Normal force gradient, 1/radian
D	Drag, lb
I	Yaw moment of inertia, slug-ft^2
S	Aerodynamic reference area, ft^2
T	Engine thrust, lb
Z	Vehicle lateral displacement, ft
a_o	Attitude error gain
a_1	Yaw rate gain, sec
b_o	Angle of attack gain
e	Distance from center of gravity to engine gimbal station, ft
f_n	Rotary undamped natural frequency, cps
l	Distance from center of gravity to center of pressure, ft
m	Mass, slugs

n	Total number of fixed engines
q	Dynamic pressure, lb/sq ft
r	Total number of control engines
t	Time from liftoff, sec
α_Q	Angle of attack, degrees
α_W	Wind angle, degrees
β	Gimbal angle, degrees
γ	Engine cant angle, degrees
ζ	Fraction of critical damping
ϕ	Attitude angle, degrees

Subscripts:

c	Control engine
f	Fixed engine
max	Maximum value

PROCEDURE

The vehicle configurations used for this study are shown in figures 1 and 2. Vehicle orientation is indicated in figure 3. Stub fins were used on the S-IA booster. The vehicle data required for the analysis are given in tables I through VIII.

The first step in the analysis was to determine the maximum gimbal angles required for control of the vehicles when flying through a two sigma yaw-plane wind. Because of the low control frequency used for the two vehicles and because of the low propellant sloshing frequencies characteristic of the vehicles, a linear control equation with time programed gains was used. It was assumed that vehicle attitude angle and angle of attack were the control variables. Path control was not included since it has little effect on the determination of maximum required gimbal angle. The control equation is given in Appendix A. Control gains were calculated using the drift minimum control principle

discussed in reference 2. The drift minimum gain variables applicable to this study are given in Appendix A. These control equations together with the equations of motion in two dimensions were programed for the IBM 7094 computer. For this study it was assumed that the quasi-steady state wind profiles peaked at maximum q and had three discrete gusts applied on top of them beyond this point. Since this was a rigid body study, a slightly conservative approach was used in obtaining the wind buildup below maximum q in that an iterative procedure was used to determine the most critical combination of wind shears to use in constructing the synthetic wind buildup profile for each of the vehicles. The vehicles were then flown into these winds and an iterative procedure used to determine the maximum gimbal angles required to prevent the vehicles from diverging.

Since this was a rigid body study made under nominal vehicle conditions and in the yaw plane only, the calculated maximum gimbal angles would not be sufficient if the effects of body flexibility, parameter tolerances, pitch plane winds, and peak winds occurring elsewhere in the trajectory were considered. The calculated gimbal angles were therefore increased an additional amount in order to approach more reasonable maximum gimbal angle values for use in the study. The resulting angle is hereafter referred to as the reduced gimbal angle. The reduced gimbal angles used in the study were considered to be quite reasonable since the percentage of reduction, for both rigid body cases, from an unrestricted gimbal angle peak to the minimum angle required to prevent divergence was 15 units greater than the percentage of reduction from the existing maximum angle to the maximum angle used in this study (also note that it is very unlikely that the gimbal angles would ever peak at their existing maximum values under balanced flight conditions).

The previously determined critical wind profiles and reduced gimbal angles were used to conduct control studies. These studies were used to determine the most critical initial conditions for divergence studies and to determine maximum balanced flight rigid body bending moments at maximum q. The escape tower mass was lumped into the command module for the bending moment calculations.

The next step in the analysis was to determine the combinations of positive angle of attack and positive hard-over-gimbal angle and the resulting bending moment distributions which would correspond to assumed structural failure of the vehicles. This was done in the manner indicated in Appendix B.

On completion of the structural failure analysis, divergence studies were run assuming hard-over negative engine failures (single failures). In order to obtain the end points on the divergence runs, it was necessary to determine the assumed break-up angles of attack for

the case of single gimbal failures. This was done by holding the gimbal angles hardover, negative, and computing bending moments for increasing angles of attack until the respective assumed break-up bending moment curves calculated previously were exceeded at some point. Locating these assumed break-up angles of attack on the divergence studies gave the end conditions for the studies. Overrate abort is presently triggered when the emergency detection system senses a pitch or yaw rate of five degrees per second; therefore, locating a yaw rate of five degrees per second on the divergence studies gave the times available for overrate abort at maximum q from each of the vehicles with their corresponding reduced gimbal angles.

A similar procedure was followed using the two vehicles with their existing maximum gimbal angles; that is, control studies to obtain divergence initial conditions, divergence studies, determination of single failure angles of attack, and finally, determination of existing available abort times. Comparison of these times with those found in the reduced angle studies indicated the relative increases in abort times to be expected as a result of reducing maximum gimbal angle travel.

The relative increase in abort times for the case of oscillatory failures was also studied. Since this case combined positive angles of attack with positive hard-over-gimbal angles, assumed break-up angles of attack were available from the structural failure analysis; therefore, the only additional step necessary was to adjust the divergence studies to reflect oscillatory gimbal failures. In order to obtain the minimum times available for abort, an iterative procedure was used to determine at what point during divergence the gimbal angles should be reversed from negative maximum in order to reach positive maximum at the same time that the vehicles were experiencing the assumed break-up angles of attack. Inserting the correct reversal times into the divergence studies gave minimum times available for abort at maximum q from each of the vehicles.

Divergence studies were run at maximum q for the case of no wind in order to show that more time is available for abort in this case.

Divergence studies were also run and load calculations made at burnout, in order to give qualitative values of abort times at that point.

RESULTS AND DISCUSSION

SATURN IB

Single Gimbal Failure

The results of the Saturn IB vehicle gimbal angle requirement study are presented in figures 4 and 5. The wind input used for this study is given in figure 6. The nominal trajectory was flown until the wind was encountered at an altitude of 20,140 feet. The gimbal angle history presented in figure 4 shows that the maximum gimbal angle required for rigid body control of the Saturn IB is 4.7°. Maximum q for the Saturn IB trajectory data used occurred at 80 seconds (the slight shifting of maximum q which occurs in the control study was ignored for purposes of wind orientation). Figure 5 shows vehicle drift and control system gains.

The 4.7° angle was increased by 1.8° resulting in a reduced gimbal angle of 6.5°. The results of a control study for this reduced angle are shown in figure 7 (the initial conditions at 78 seconds were taken from fig. 4). Figure 7 indicates that the most critical time for divergence initiation is 80.1 seconds. Initial conditions at this time were therefore used as a basis for the divergence study shown in figure 8.

The maximum balanced flight bending moment curve was evaluated using the results of the control study (fig. 7) and is shown in figure 9 as the curve for 6.5° gimbal angle and 7.93° angle of attack. However, this bending moment curve was not used to calculate an assumed peak failure point since its corresponding gimbal angle was slightly clipped (fig. 7). A special control study (not shown) for a maximum gimbal angle of 8° was run and a corresponding maximum balanced flight bending moment curve (not shown) was computed. This curve together with the longitudinal load curve at 80 seconds in figure 10 was used to calculate the assumed peak failure point of $740\ (10)^5$ in.-lb shown in figure 9.

The divergence curves are shown on figure 8, for the 6.5° angle, as solid lines up to 81.22 seconds and as dashed lines beyond 81.80 seconds, and on figure 11, for the 8° angle, as solid lines up to 81.13 seconds and as dashed lines beyond 81.80 seconds. The sections between the times noted are omitted for clarity. A hard-over-gimbal rate of 23.6° per second was used for the divergence studies. The initial conditions for figure 11 were obtained from the special 8° control study mentioned above. Note that the principal difference in initial conditions between figures 8 and 11 is the 0.5° increase in initial gimbal angle.

The angles of attack at which assumed failures occur when the gimbal angles are hardover at -6.5° and -8° were obtained from figures 9 and 12, respectively, as indicated in the "Procedure" section and were found to be 20.9° and 21.4°, respectively. The assumed failure bending moment curves for these cases are not shown, but they would appear in the manner indicated by the dashed curve in figures 20 and 23.

Figures 8 and 11 show that assumed failure occurs at 82.01 seconds for the reduced angle and at 82.04 seconds for the existing angle. (The slight decrease in time to assumed failure resulting from the reduced angle stems from the lower break-up angle of attack and the smaller initial gimbal angle as shown on fig. 8.) The figures also show that overrate abort sensing occurs at 80.96 seconds for the reduced angle and at 80.99 seconds for the existing angle; therefore, there is no increase in time available for abort for this case.

Oscillatory Failure

Interpolation between the curves of figure 9 gave an assumed break-up bending moment curve corresponding to a positive gimbal angle of 6.5° and an angle of attack of 16.6°. Figure 8 shows this combination of angles occurring at 81.8 seconds; that is, at a divergence time of 1.7 seconds.

Interpolation between the curves of figure 12 gave an assumed break-up bending moment curve corresponding to a positive gimbal angle of 8° and an angle of attack of 15.9°. Figure 11 shows this combination of angles occurring at 81.8 seconds, resulting in a divergence time of 1.7 seconds.

The principal reason figure 8 shows no increase in time to failure is that, due to the different initial conditions, gimbal angle reversal for this 6.5° case leads that of figure 11 for the 8° case up to 80.64 seconds. However, even if the initial conditions were the same, there would be negligible difference in time to failure between the two cases since the angles of attack at assumed break-up are very similar.

Figures 8 and 11 show that overrate abort sensing occurs at 80.96 seconds for the reduced angle and at 80.99 seconds for the existing angle; therefore, there is only a 0.04 second increase in time available for abort for this case.

Zero Wind

The results of the divergence studies at maximum q for no wind are presented in figure 13. These results indicate that more time is required to reach a given angle of attack in the case of divergence

directly from the nominal Saturn IB trajectory (no wind). This means, of course, that more time would be required to reach a specified break-up bending moment distribution, resulting in more time available for abort since there is very little difference in abort sensing time between this case and the two sigma wind case.

Burnout

The results of the study at burnout using the reduced angle are shown in figures 9 and 14. The assumed peak failure point of $380\ (10)^5$ in.-lb shown on figure 9 was calculated from the longitudinal load at 145 seconds since the four fixed engines are shutdown after this time. The burnout bending moment shown in figure 9 increased only slightly from 145 to 150 seconds, consequently, this moment was calculated at 150 seconds in order to present a slightly conservative study at 145 seconds. Since atmospheric density was considered negligible at burnout, the bending moment does not increase after the gimbal angle reaches 6.5°, consequently, figure 9 indicates that there is no limit on available abort time, as far as booster break-up is concerned, for the reduced angle case. The true failure point at burnout, however, may deviate considerably from that shown on figure 9 and may, of course, fall within the bending moment envelope. If this condition should exist, break-up will occur within 0.27 second after initiation of an engine hard-over condition. Note that, in this case, the overrate abort system would not sense an abort situation before break-up occurred. There is a definite need for further study of burnout abort when sufficient structural data becomes available, particularly since the bending moment envelope for the existing gimbal angle is larger than that for the reduced angle.

SATURN V

Single Gimbal Failure

Results of the Saturn V vehicle gimbal angle requirement study are presented in figures 15 and 16. The wind input for this study is given in figure 17. The nominal trajectory was flown until the wind was encountered at an altitude of 18,980 feet. The gimbal angle history in figure 15 shows that the maximum gimbal angle required for rigid body control of the Saturn V vehicle is 0.7°. Maximum q for the Saturn V trajectory data used occurred at 72 seconds. Figure 16 shows vehicle drift and control system gains.

The 0.7° angle was increased by 2.3° resulting in a reduced gimbal angle of 3°. The results of a control study for this reduced

angle are shown in figure 18. These results indicate that the most critical time for divergence initiation is 72.1 seconds; therefore, the divergence study (fig. 19) used the initial conditions at this time.

The maximum balanced flight bending moment curve was evaluated using the results of the control study (fig. 18) and is shown in figure 20. This bending moment curve (since the gimbal angle peaked below 3° in fig. 18) and the longitudinal load curve at 72 seconds shown in figure 21 were used to calculate the assumed peak failure point of 505 $(10)^6$ in.-lb shown in figure 20. The burnout assumed peak failure point of 130 $(10)^6$ in.-lb was calculated from the longitudinal load at 144 seconds.

The divergence curves for this case are shown on figure 19, for the reduced angle, as solid lines up to 74.3 seconds and as dashed lines beyond 74.9 seconds, and on figure 22, for the existing angle, as solid lines up to 73.05 seconds and as dashed lines beyond 74.05 seconds. The sections between the times noted are omitted for clarity. A hard-over-gimbal rate of 10 degrees per second was used for the divergence studies. Figure 18 was used for the initial conditions in the existing case also, since the gimbal angle peaked below 3°.

The angles of attack at which assumed failures occur when the gimbal angles are hardover at -3° and -5.15° were obtained from figures 20 and 23, respectively. The assumed failure bending moment curves are shown dashed on the figures.

Figures 19 and 22 show that assumed failure occurs at 75.60 seconds for the reduced angle and at 75.10 seconds for the existing angle. The figures also show that overrate abort sensing occurs at 73.62 seconds for the reduced angle and at 73.30 seconds for the existing angle; therefore, there is a 0.18 second increase in time available for abort for this case.

Oscillatory Failure

Interpolation between the curves of figure 20 gave an assumed break-up bending moment curve corresponding to a positive gimbal angle of 3° and an angle of attack of 19.1°. Figure 19 shows this combination of angles occurring at 74.90 seconds; that is, at a divergence time of 2.80 seconds.

Interpolation between the curves of figure 23 gave an assumed break-up bending moment curve corresponding to a positive gimbal angle of 5.15° and an angle of attack of 13.8°. Figure 22 shows this

combination of angles occurring at 74.05 seconds, resulting in a divergence time of 1.95 seconds.

Figures 19 and 22 show that overrate abort sensing occurs at 73.62 seconds for the reduced angle and at 73.37 seconds for the existing angle; therefore, there is a 0.60 second increase in time available for abort for this case.

Zero Wind

Results of divergence studies at maximum q for no wind are presented in figure 24. These results indicate that more abort time is available in the case of divergence directly from the nominal Saturn V trajectory (no wind).

Burnout

The burnout bending moment for the reduced angle case is shown on figure 20. Figures 20 and 25 indicate that structural failure may occur before the engines reach the hardover position; that is, within 0.3 second after initiation of an engine hardover condition. This result indicates the extreme desirability (when actual break-up loads become available) of further study of burnout abort.

CONCLUDING REMARKS

The present rigid body, yaw plane analysis at maximum q has shown that only small increases in abort times are obtained by reducing the existing Saturn IB and Saturn V maximum allowable engine gimbal angles. A more comprehensive analysis including body flexibility, headwind and tailwind pitch plane failures, accurate structural data, et cetera, would probably lead to even shorter abort times in some cases. It is therefore concluded that no significant abort time increases can be realized under design wind conditions at maximum q in the case of single failure of either of the two vehicles.

Oscillatory failure was primarily presented as a hypothetical "worst case"; however, if it should be a consideration in the Apollo-Saturn V mission analysis, the possibility of Saturn V maximum gimbal angle reduction would warrant further consideration. Abort time increase in the case of Saturn IB oscillatory failure was insignificant.

The burnout abort study served to give some insight into the problem of abort during booster burnout. The study indicated that structural failure could occur even before the engines reach the hardover position. Further study of available burnout abort time should be made when actual structural data becomes available.

REFERENCES

1. "Natural Environment and Physical Standards for Project Apollo." (U) M-DE 8020.008A, Office of Manned Space Flight, NASA, Headquarters. CONFIDENTIAL

2. Hoelker, R. F.: "The Principle of Artificial Stabilization of Aerodynamically Unstable Missiles," ABMA DA-TR-64-59, September 25, 1959. CONFIDENTIAL

3. Saturn I-B Air Load Manual. Aeroballistics Division, GSFC, April 1963.

4. "C-5 Launch Vehicle Design Data." IN-P&VE-V-62-6, Propulsion and Vehicle Engineering Division, GSFC, December 1962. CONFIDENTIAL

5. Saturn V Three Stage to Escape (LOR) Air Load Manual. Aeroballistics Division, GSFC, October 1962.

APPENDIX A

Vehicle Control Equations

The idealized control equation used for this yaw plane study is

$$\beta = a_o \phi + a_1 \dot{\phi} + b_o \alpha_Q \tag{1}$$

The drift minimum control gains are given by

$$b_o = \frac{4\pi^2 f_n^2 \left(K_2 + \frac{C_1}{C_2} K_3\right) + C_1 \left(K_2 + \frac{C_1}{C_2} K_3 + K_1\right)}{C_2 \left(K_1 + K_2\right) + C_1 K_3} \tag{2}$$

$$a_o = \frac{4\pi^2 f_n^2 + C_1}{C_2} - b_o \tag{3}$$

$$a_1 = 2l \sqrt{\frac{C_2 \left(a_o + b_o\right) - C_1}{C_2}} \tag{4}$$

where

$$C_1 = \frac{C_{N_\alpha} q S l}{I} \tag{5}$$

$$C_2 = \frac{erT_c \cos \gamma_c}{I} \tag{6}$$

$$K_1 = \frac{rT_c \cos \gamma_c + nT_f \cos \gamma_f - D}{m} \tag{7}$$

$$K_2 = \frac{C_{N_\alpha} q S}{m} \tag{8}$$

$$K_3 = \frac{rT_c \cos \gamma_c}{m} \tag{9}$$

for the vehicles considered and for the assumptions made in this study.

APPENDIX B

Procedure for Determining Assumed Break-Up Bending Moment Curves and Corresponding Angles of Attack

Actual break-up loads were not available for use in this study; therefore, arbitrarily large assumed vehicle break-up bending moments for divergence comparison purposes were evaluated by considering longitudinal loads and maximum balanced flight bending moments (using the existing gimbal angles) only and using a safety factor of 1.4 based on material ultimate strength. Assumed peak failure points were calculated in this manner for both vehicles. The remainder of the assumed break-up curve for each vehicle was considered to follow the trend established by the balanced flight curve; that is, positive angle-of-attack and gimbal angle.

Figure 26 shows an assumed break-up curve at maximum q for the Saturn V vehicle. The maximum balanced flight bending moment curve shown in figure 20 and the longitudinal load curve at 72 seconds shown in figure 21 were used to calculate the assumed peak failure point of $505\ (10)^6$ in.-lb shown on figure 26. The engines were then held hard-over positive at 5.15° and bending moments were computed for angles of attack of 10, 15 and 20 degrees. The bending moments were then plotted on figure 26. Interpolation between these curves gave the remainder of the assumed break-up curve shown on figure 26. An angle-of-attack interpolation between the peak points on the curves indicated that the assumed break-up curve would result from an angle of attack of 13.8°.

The approximation of break-up loads is, of course, extremely crude but probably introduced little error into the study, since relative, not absolute, divergence times were the desired result.

TABLE I.- SATURN IB TRAJECTORY DATA[a]

Time from liftoff, sec	Thrust, lb	Drag, lb	Velocity, fps	Altitude, ft
60	1,594,783	85,796	755	17,870
64	1,606,525	96,715	844	20,975
68	1,618,128	143,781	941	24,405
72	1,629,305	217,127	1,034	28,154
76	1,639,779	245,542	1,130	32,201
80	1,649,341	246,545	1,233	36,545
84	1,657,795	226,082	1,349	41,200
88	1,664,987	200,178	1,480	46,191
92	1,671,012	172,092	1,627	51,545
150	940,612	---	5,760	187,580

[a]Obtained from a 100 nautical mile circular orbit computer run made by Mission Analysis Section on December 28, 1962.

TABLE II.- SATURN IB MASS CHARACTERISTICS[a]

Time from liftoff, sec	Center of gravity, in. (b)	Mass, slugs	Yaw moment of inertia, slug-ft^2
60	727	28,486	53.4×10^6
70	737	26,653	53.3
80	752	24,820	52.7
90	770	22,986	51.8
100	797	21,153	50.5
150	1,113	12,400	28.8

[a]Obtained from curves prepared by Design Integration Section, Flight Vehicle Integration Branch, on February 8, 1963.

[b]Measured from vehicle station 0.

TABLE III.- SATURN IB STATIC LONGITUDINAL STABILITY

[From ref. 3]

Mach number	Normal force gradient, 1/radian	Center of pressure, in. (a)
0.75	3.667	1,223
0.85	3.724	1,208
1.00	3.782	1,179
1.20	3.839	1,195
1.40	3.896	1,218
1.60	3.953	1,233
2.00	4.125	1,275
2.50	4.297	1,326
3.00	4.240	1,393

[a]Measured from vehicle station 0.

TABLE IV.- SATURN IB NORMAL
FORCE DISTRIBUTION AT A MACH NUMBER OF 1.274

[From ref. 3]

Center of pressure, in. (a)	Normal force gradient, 1/radian	Non-linear normal force coefficient
2,325	---	$0.405 \times 2 \sin^3\alpha_Q$
2,325	0.461	---
2,257	.687	---
2,109	---	1.231
1,834	---	.744
1,795	.344	---
1,756	.747	---
1,574	---	2.340
1,181	---	2.250
796	---	2.250
363	---	2.810
130	1.699	---

[a]Measured from vehicle station 0.

TABLE V.- SATURN V TRAJECTORY DATA[a]

Time from liftoff, sec	Thrust, lb	Drag, lb	Velocity, fps	Altitude, ft
52	8,023,934	231,695	776	16,248
56	8,097,315	268,029	879	19,382
60	8,170,147	387,083	990	22,859
64	8,240,700	470,646	1,109	26,682
68	8,307,413	499,437	1,238	30,854
72	8,369,010	492,354	1,378	35,381
76	8,423,496	452,916	1,532	40,271
80	8,469,721	403,129	1,701	45,532
84	8,507,900	350,961	1,885	51,174
150	6,904,739	---	7,567	205,828

[a]Obtained from a "three stage to escape" computer run made by Mission Analysis Section on June 27, 1963.

TABLE VI.- SATURN V MASS CHARACTERISTICS

[From ref. 4]

Time from liftoff, sec	Center of gravity, in. (a)	Mass, slugs	Yaw moment of inertia, slug-ft^2
50	1,220	142,267	6.02×10^8
60	1,230	133,423	5.92
70	1,255	124,579	5.80
80	1,280	115,735	5.68
90	1,308	106,891	5.50
150	1,845	54,697	3.00

[a]Measured from vehicle station 0.

TABLE VII.- SATURN V STATIC LONGITUDINAL STABILITY

[From ref. 5]

Mach number	Normal force gradient, 1/radian	Center of pressure, in. (a)
0.5	4.670	1,423
0.8	5.120	1,280
1.0	5.480	1,256
1.2	5.350	1,316
1.4	5.042	1,446
1.7	4.526	1,593
2.0	4.297	1,704
2.5	4.183	1,827
3.0	4.125	1,890
3.5	4.068	1,894

[a]Measured from vehicle station 0.

TABLE VIII.- SATURN V NORMAL FORCE DISTRIBUTION AT A MACH NUMBER OF 1.4

[From ref. 5]

Center of pressure, in. (a)	Normal force gradient, 1/radian	Non-linear normal force coefficient
3,797	---	$0.111 \times \sin^3 \alpha_Q$
3,792	0.213	---
3,678	---	.296
3,642	.131	---
3,519	.040	---
3,500	---	.370
3,355	.115	---
3,319	---	.378
3,280	.215	---
3,193	---	.900
3,125	.208	---
2,998	.135	---
2,846	---	.750
2,823	.040	---
2,637	.224	---
2,613	---	.855
2,548	.282	---
2,406	.564	---
2,304	---	2.035
2,161	.518	---
1,904	.118	---
1,896	---	1.920
1,621	-.034	---
1,500	---	1.920
1,421	-.026	---
1,104	---	1.920
708	---	1.920
300	---	2.035
144	1.064	---
124	1.490	---

[a] Measured from vehicle station 0.

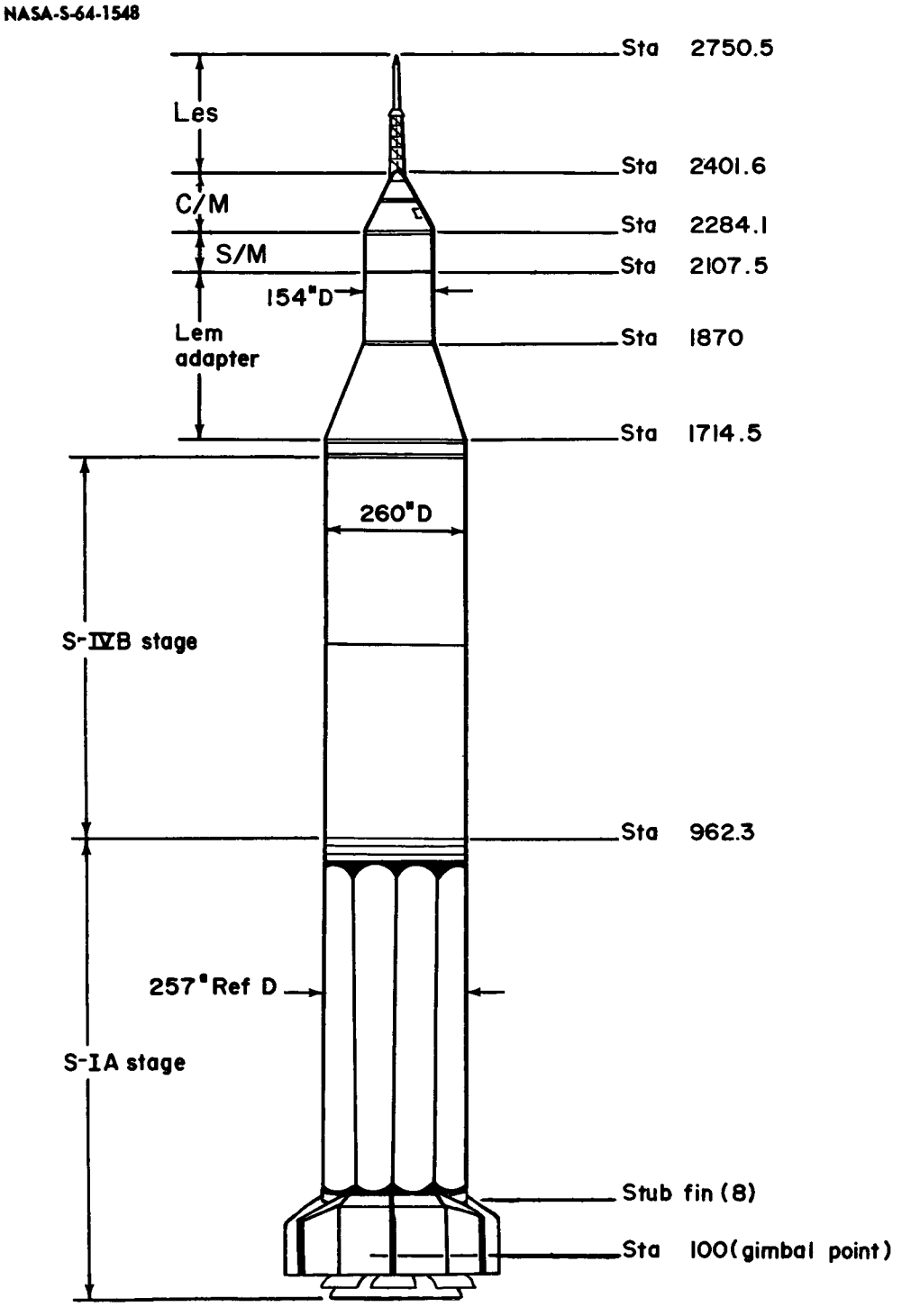

Figure 1 - Apollo /Saturn IB launch configuration

NASA-S-64-1549

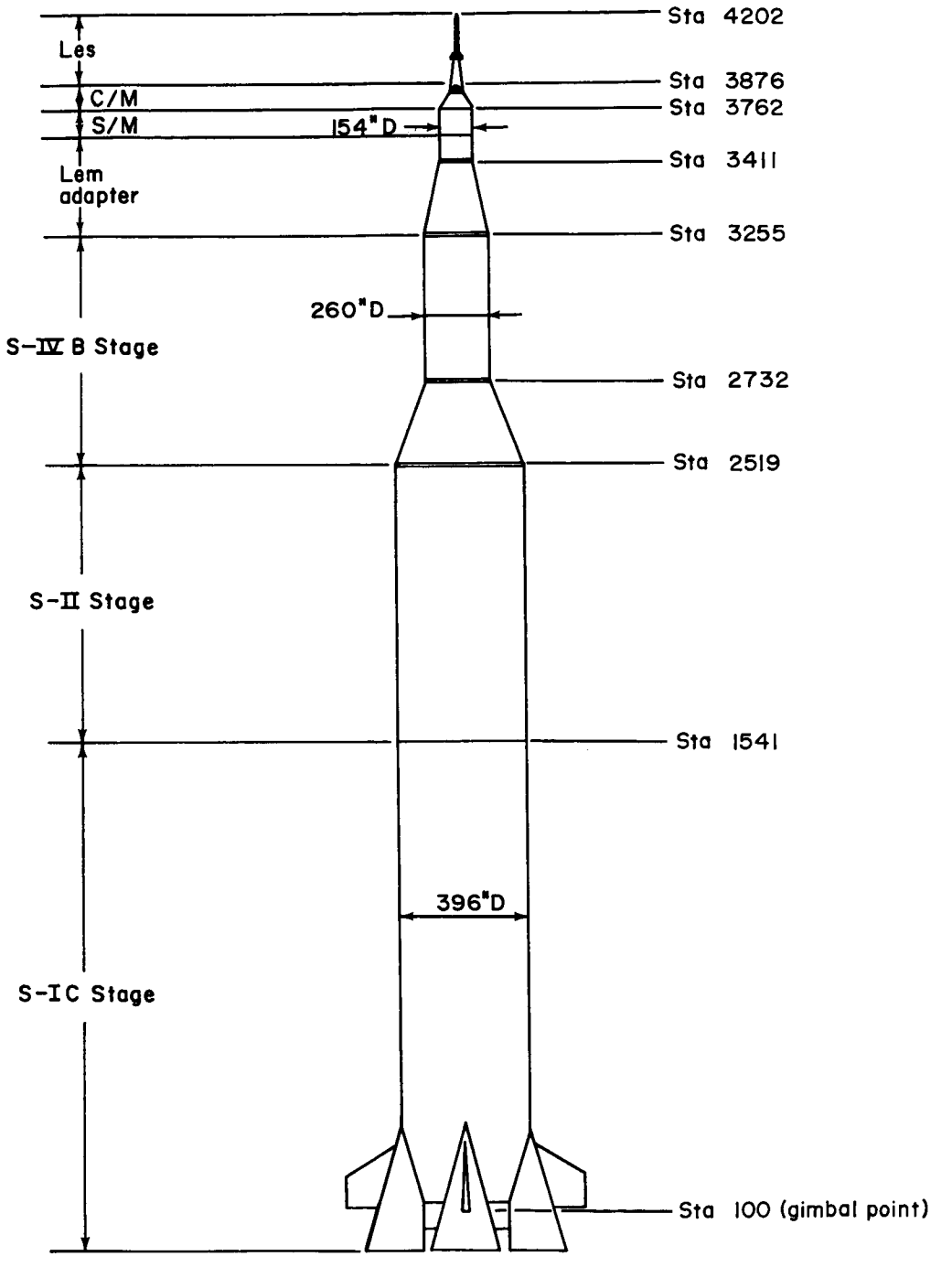

Figure 2 - Apollo/Saturn V launch configuration

NASA-S-64-1564

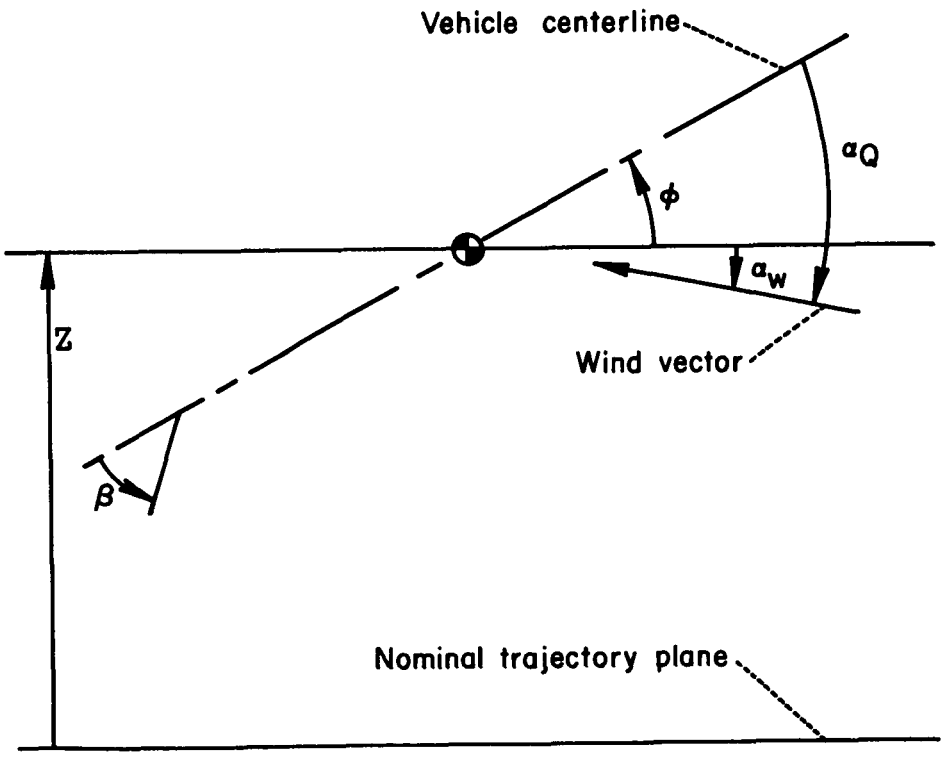

Figure 3 – Yaw plane angles and displacement

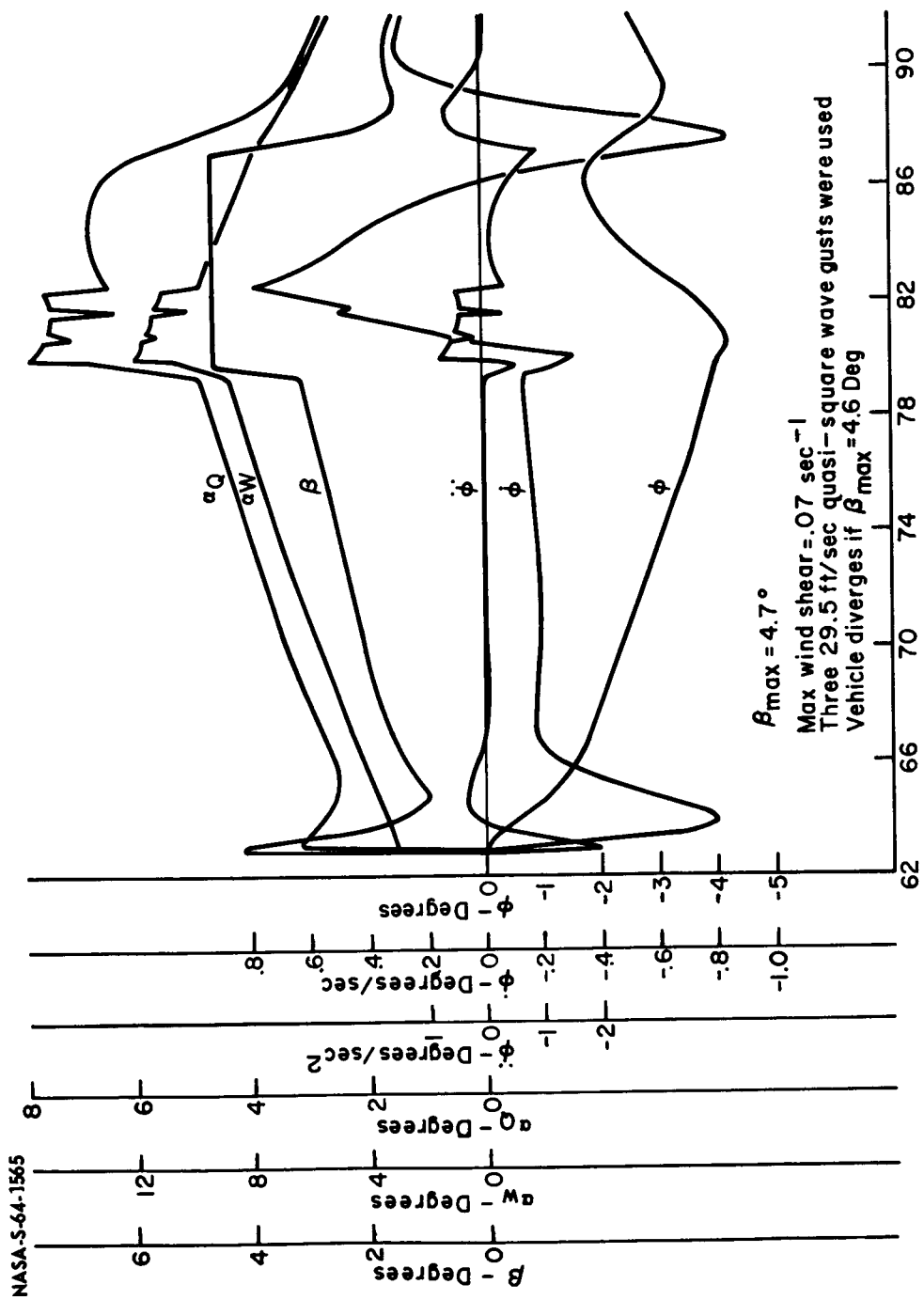

Figure 4 -Apollo/Saturn IB (withLEM) control response to 95% probability level wind profile

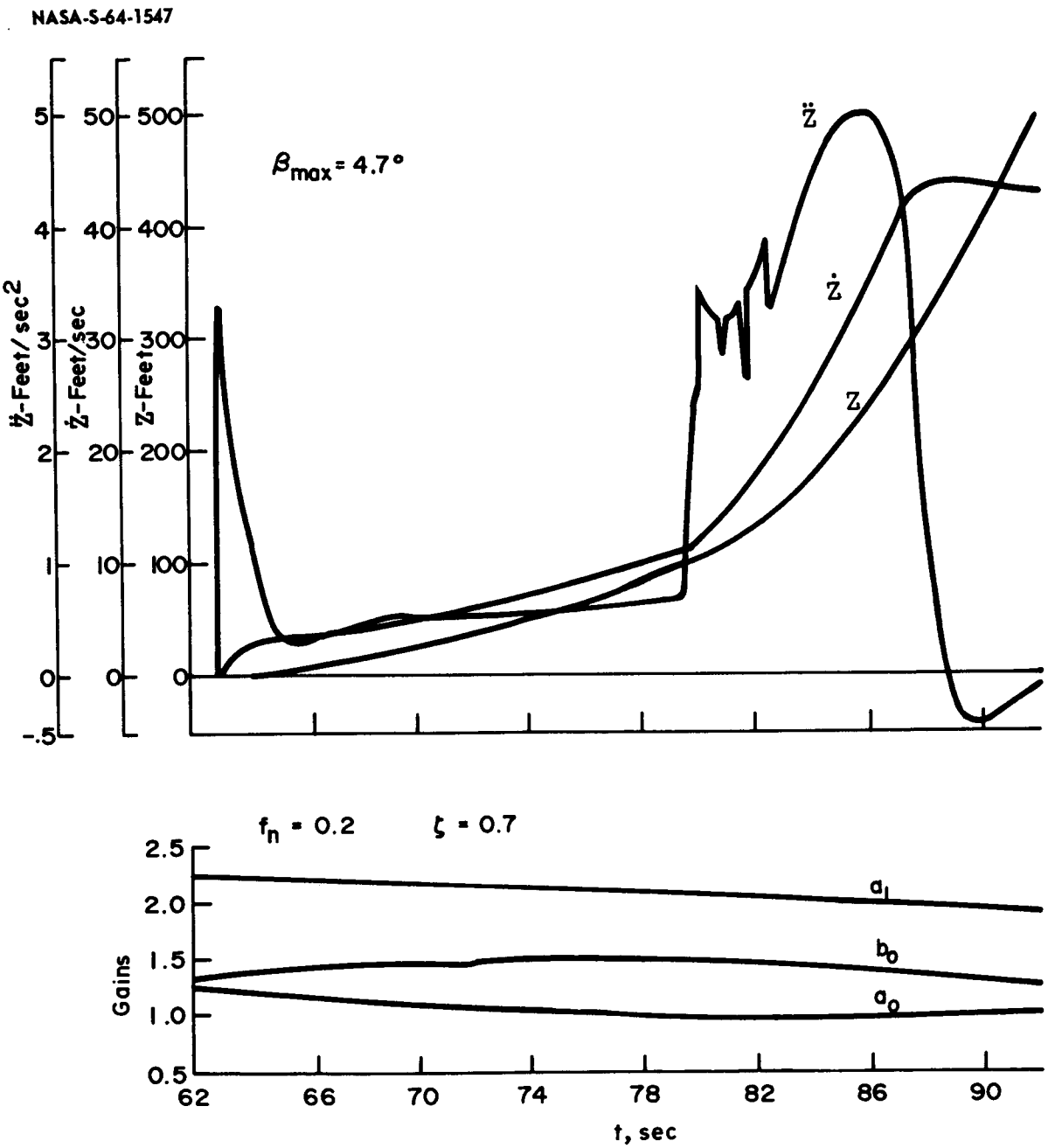

Figure 5 -Apollo/Saturn IB (with LEM) vehicle lateral motion & gains- 95% probability level wind profile

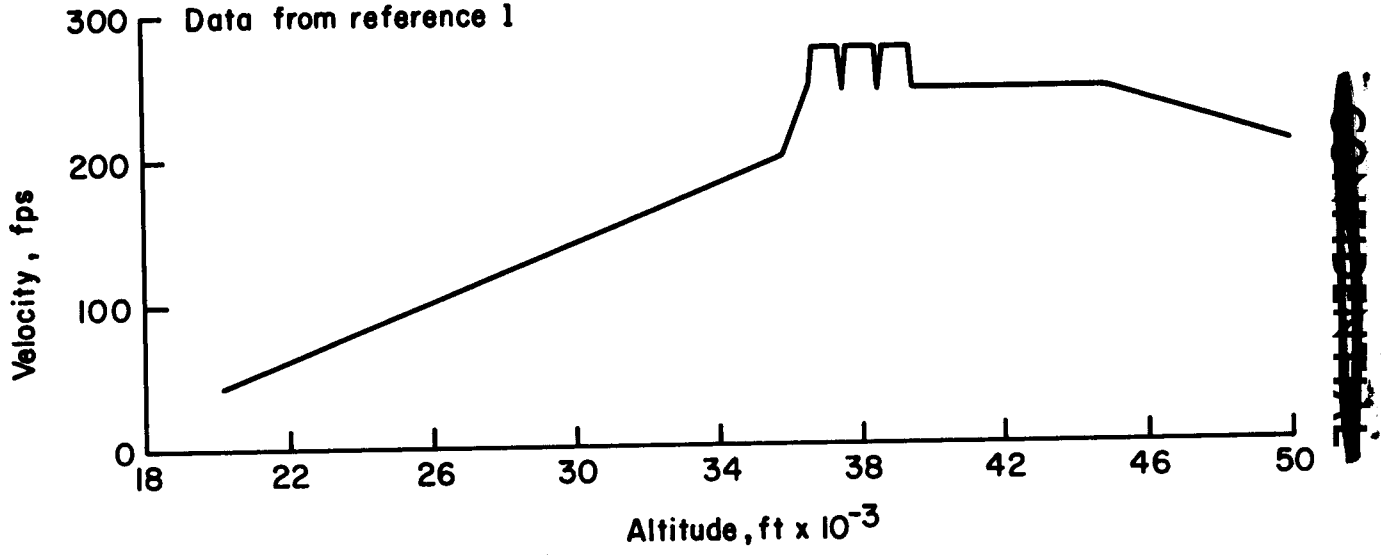

Figure 6 – Saturn IB wind input

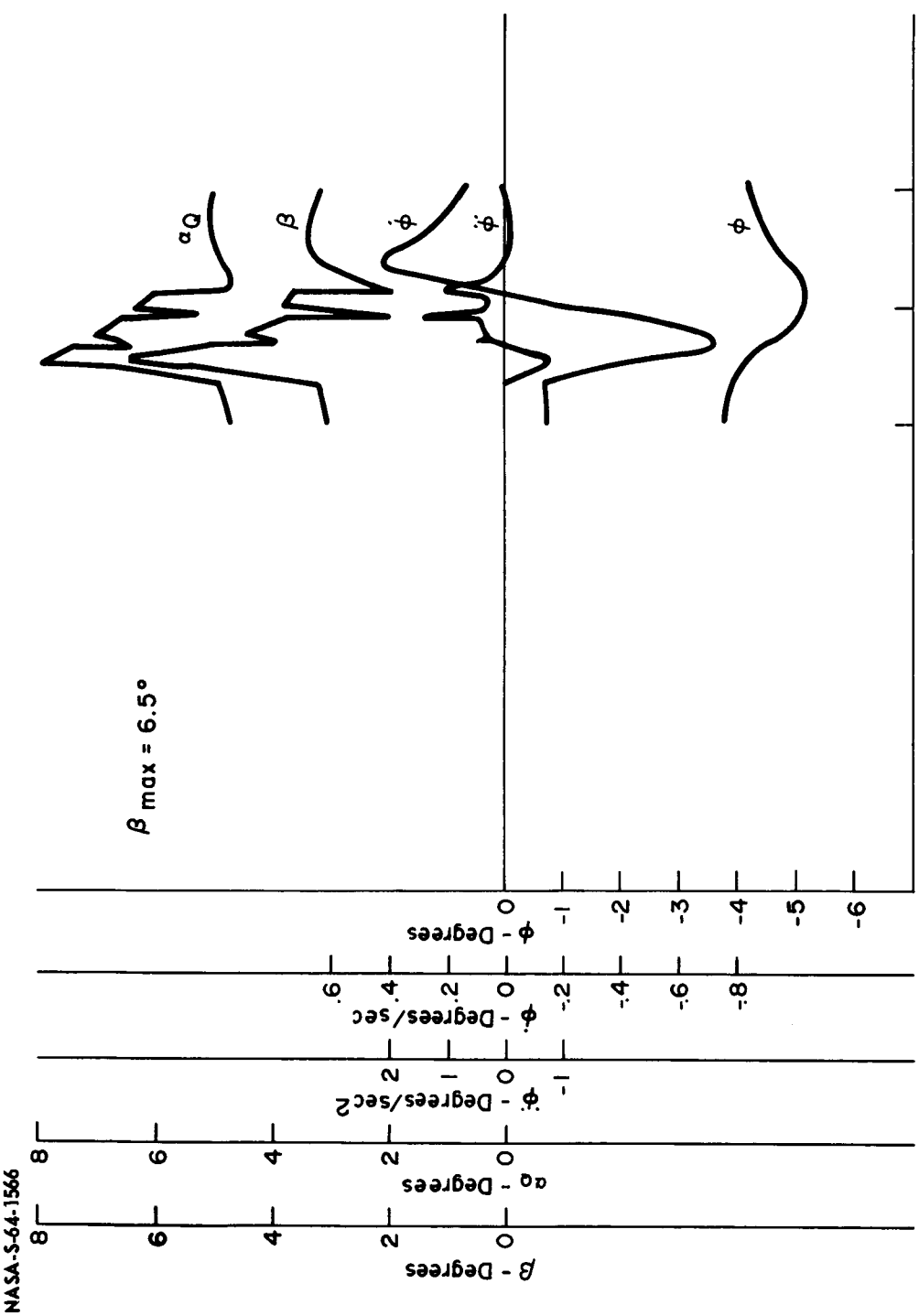

Figure 7 -Apollo/Saturn IB (with LEM) control response to 95% probability level wind profile

~~CONFIDENTIAL~~

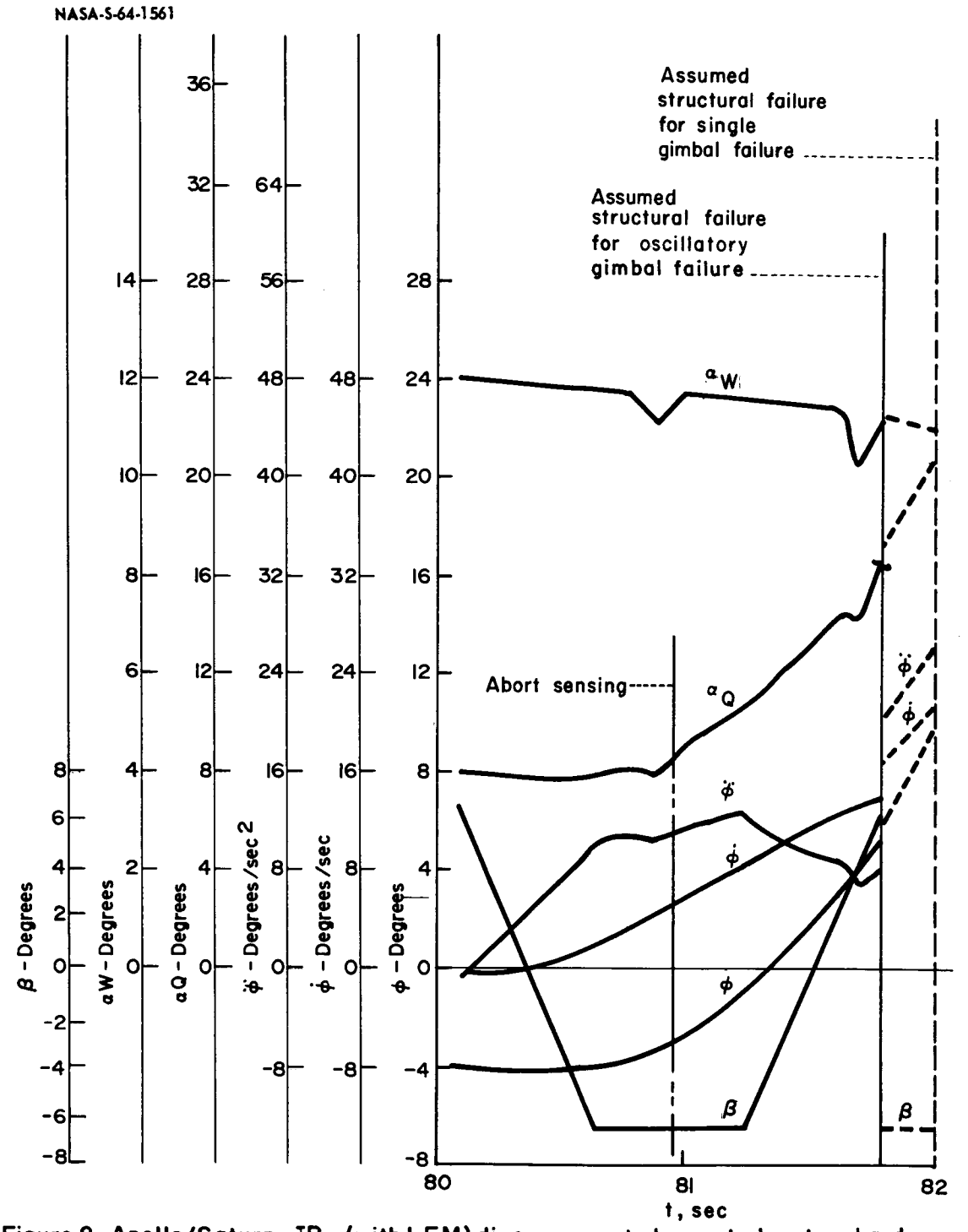

Figure 8 -Apollo/Saturn IB (with LEM) divergence study-control motors hard over at q_{max}

~~CONFIDENTIAL~~

NASA-S-64-1560

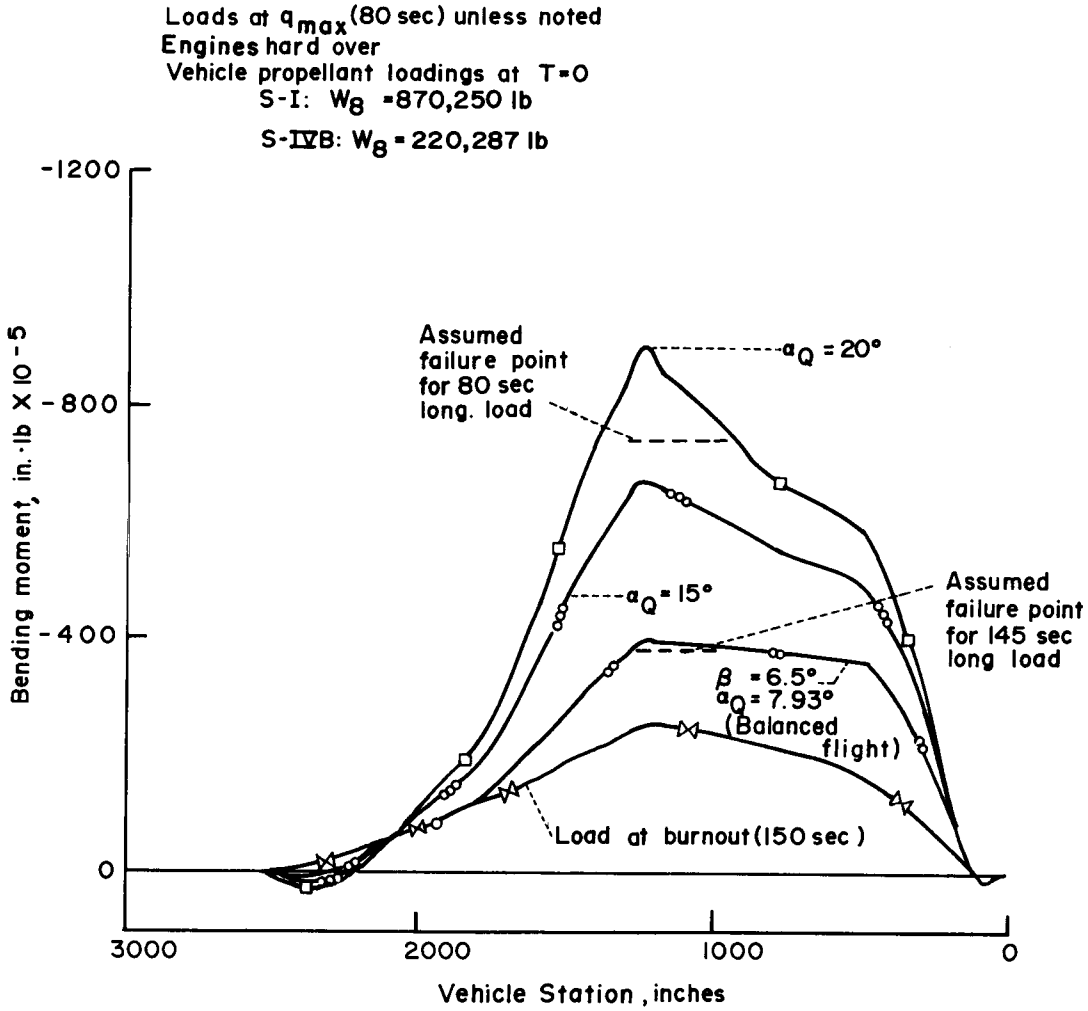

Figure 9 - Apollo/Saturn IB (with LEM) expected bending moment distributions

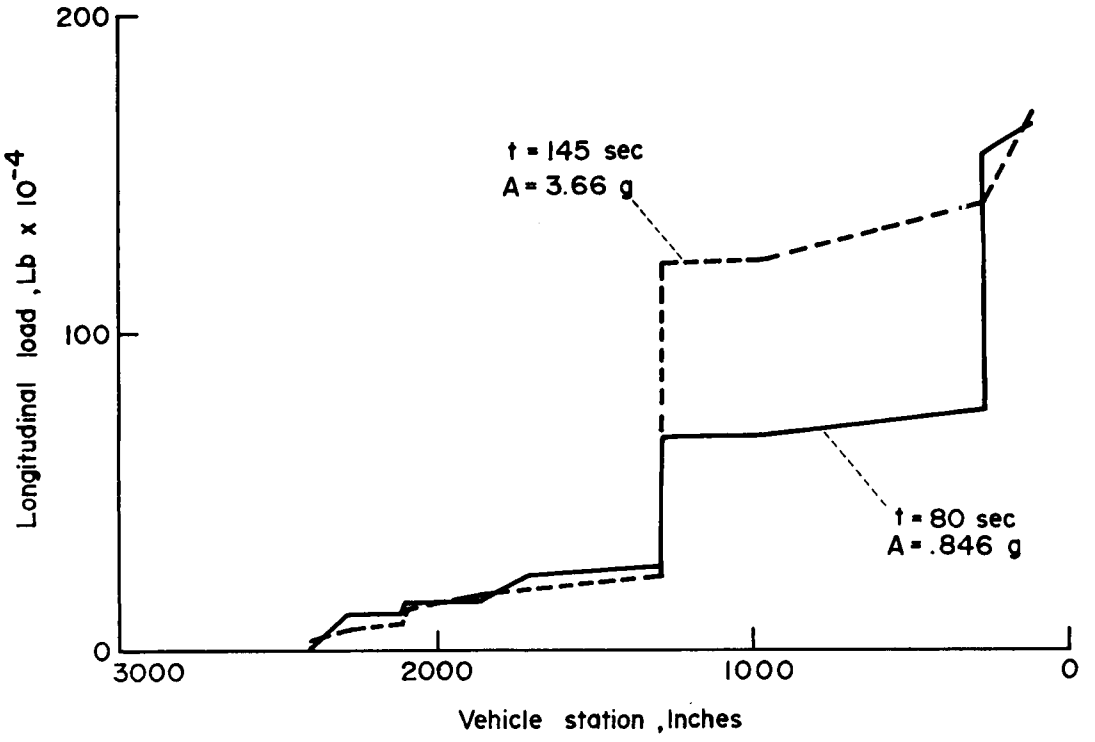

Figure 10-Apollo/Saturn IB (with LEM) longitudinal load distributions

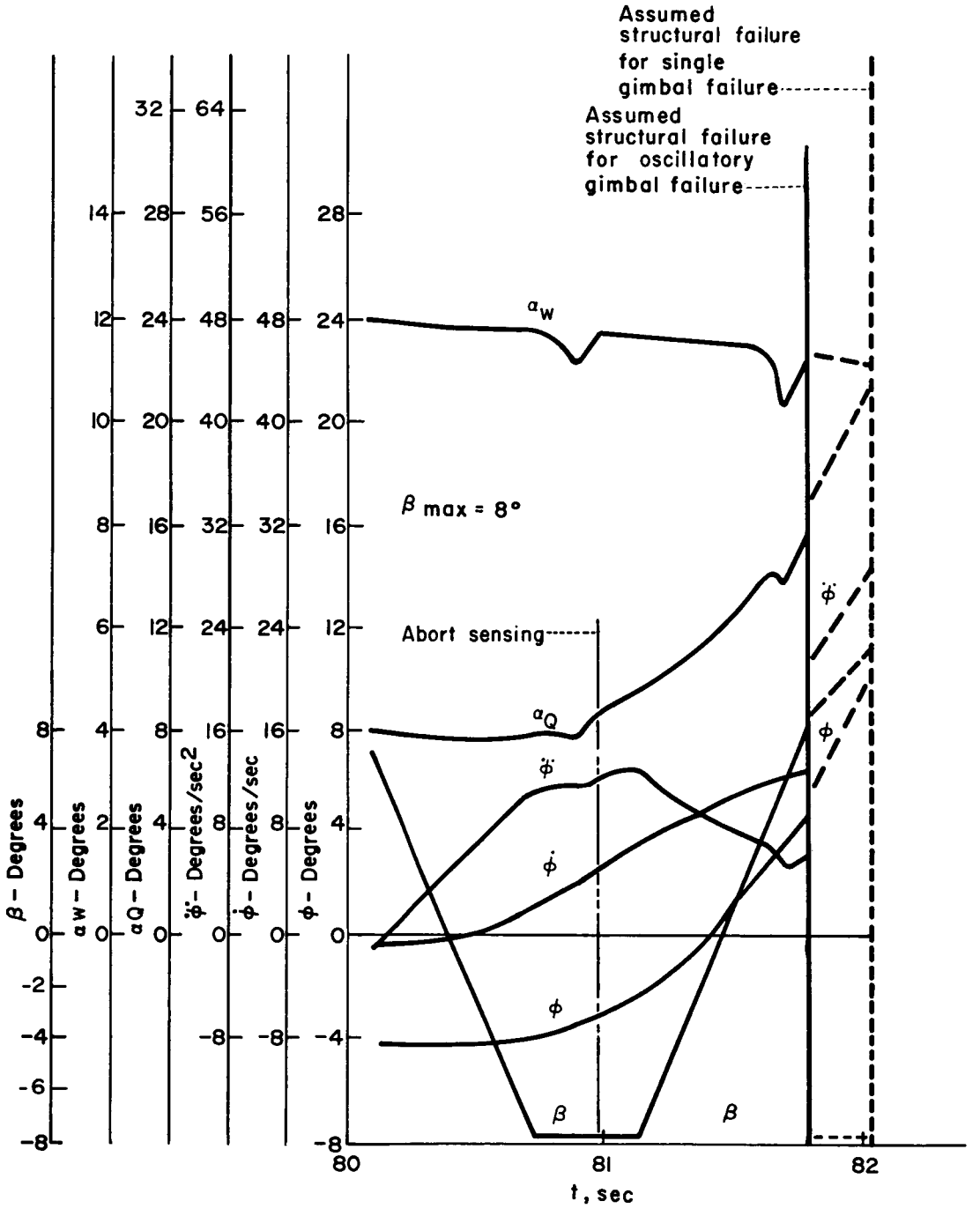

Figure 11 -Apollo/Saturn IB (with LEM) divergence study- control motors hard over at q_{max}

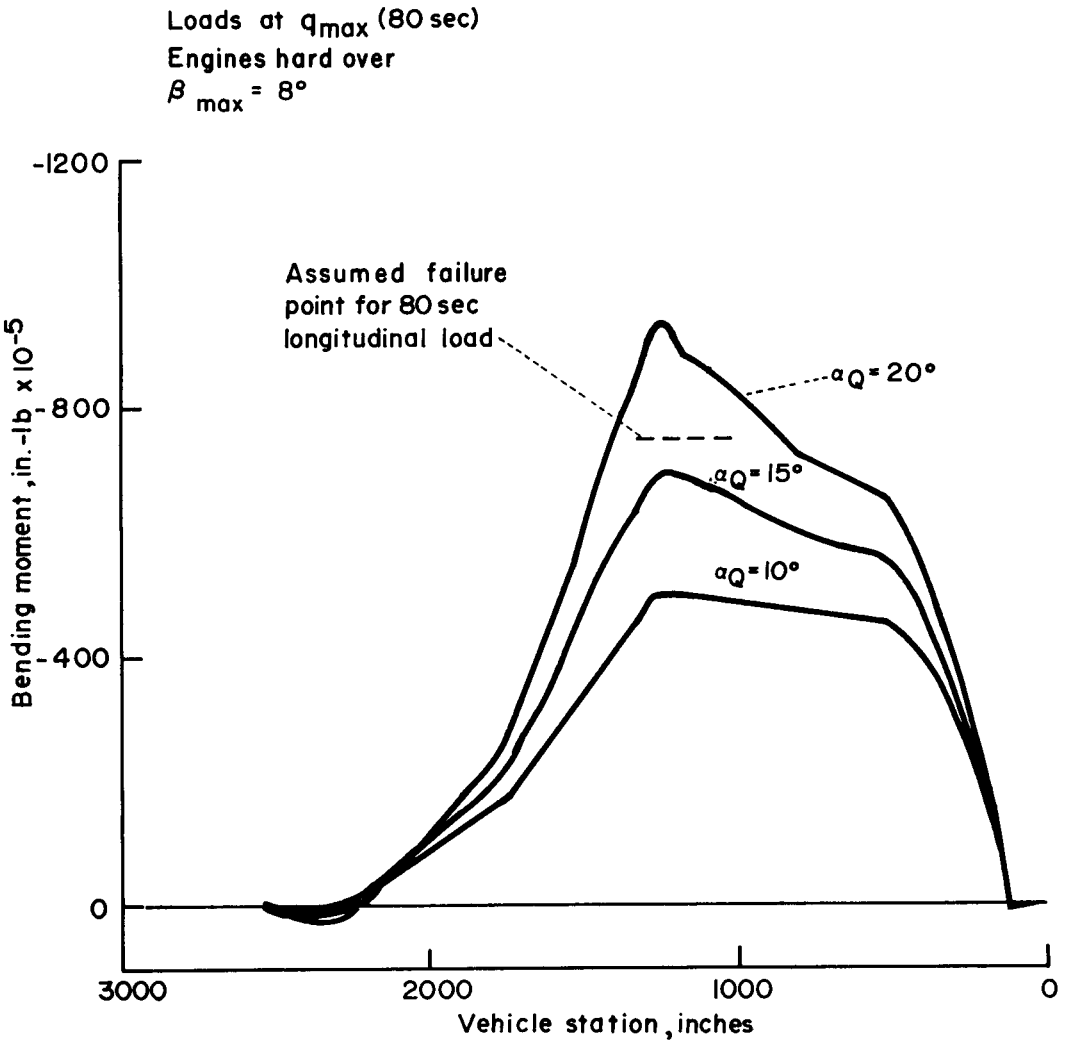

Figure 12 - Apollo/Saturn IB (with LEM) expected bending moment distributions

NASA-S-64-1567

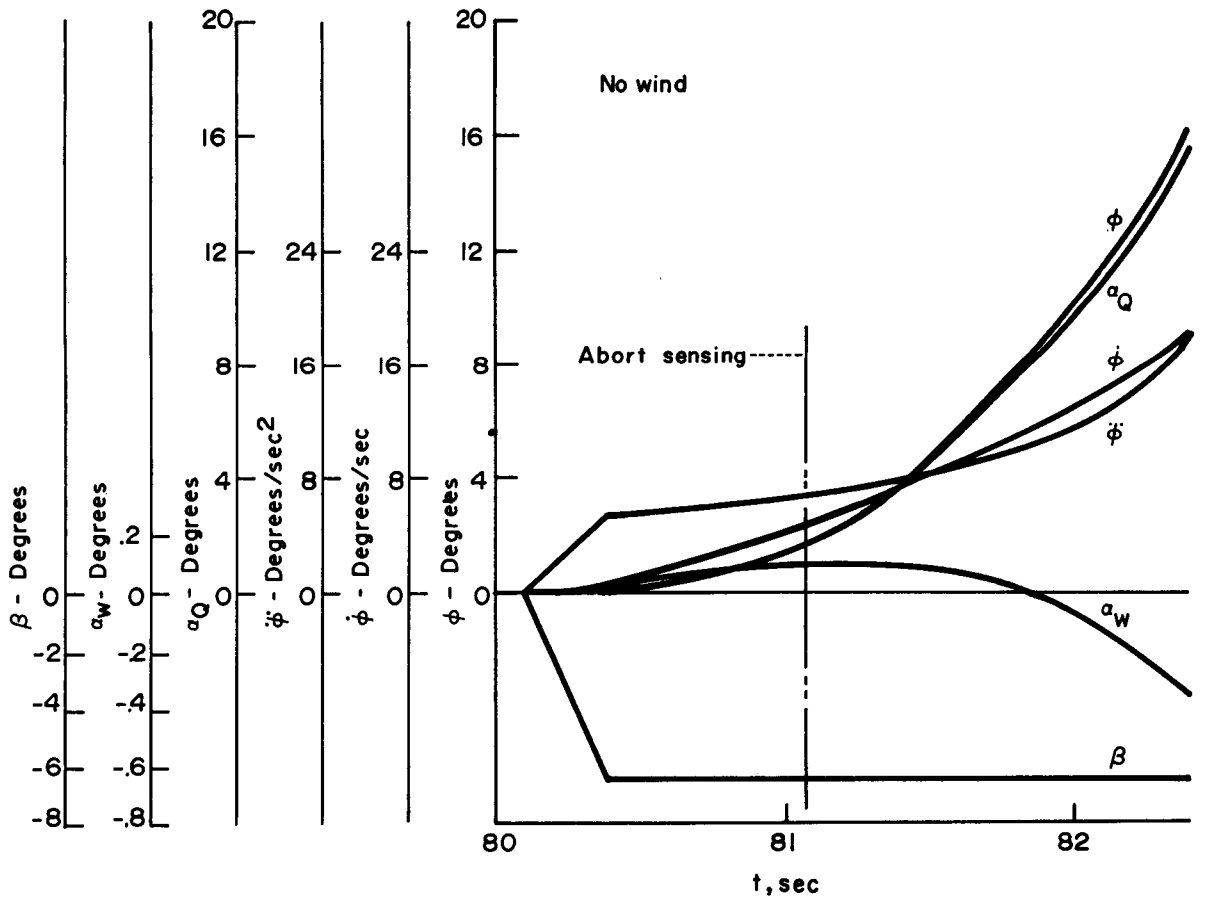

Figure 13 -Apollo/Saturn IB (with LEM) divergence study - control motors hard over at q_{max}

~~CONFIDENTIAL~~

NASA-S-64-1562

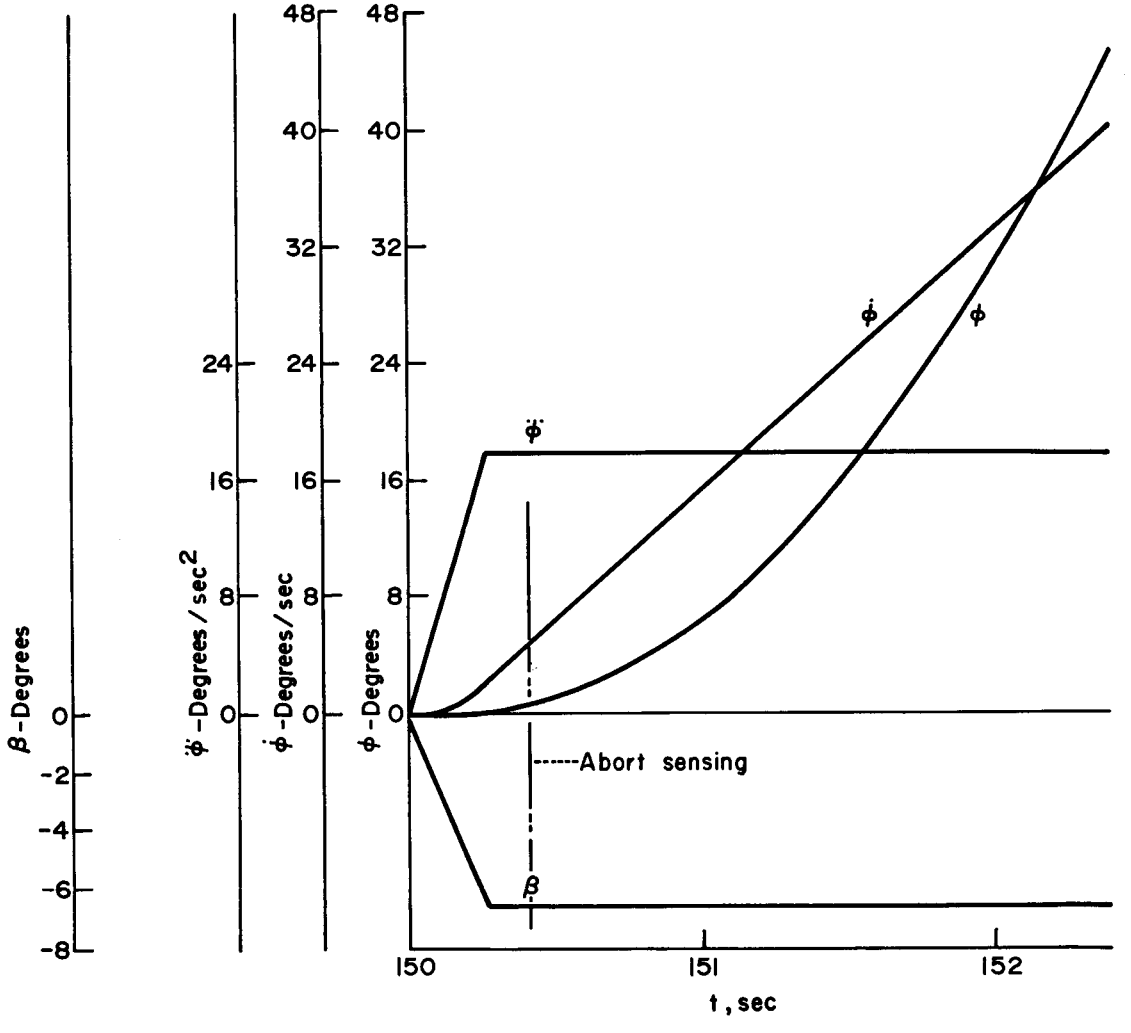

Figure 14 - Apollo/Saturn IB divergence study-control motors hard over at burnout

~~CONFIDENTIAL~~

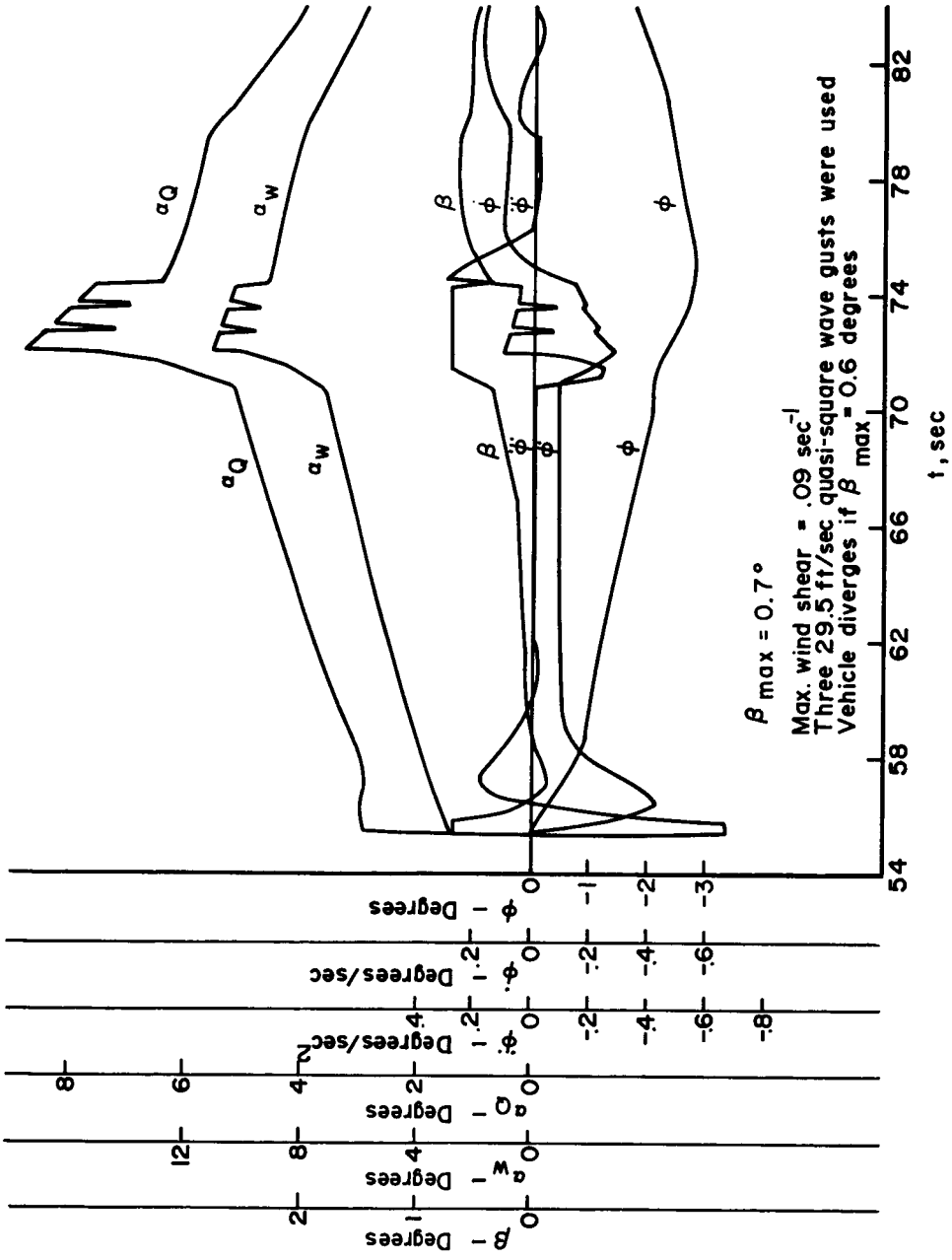

Figure 15- Saturn V control response to 95 % probability level wind profile

NASA-S-64-1572

S-64-1559

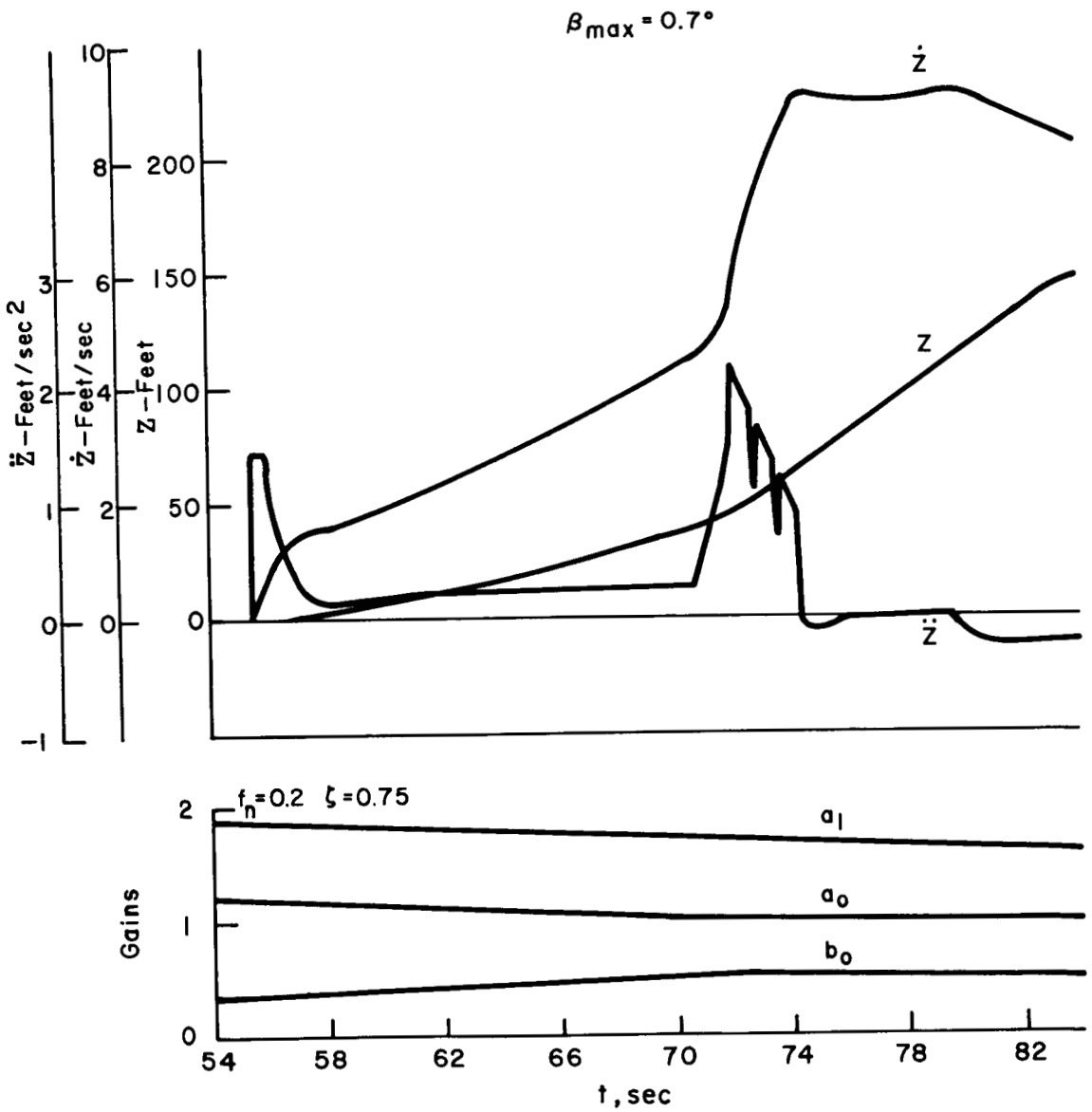

Figure 16-Saturn V lateral motion & gains
95% probability level wind profile

Data from reference 1

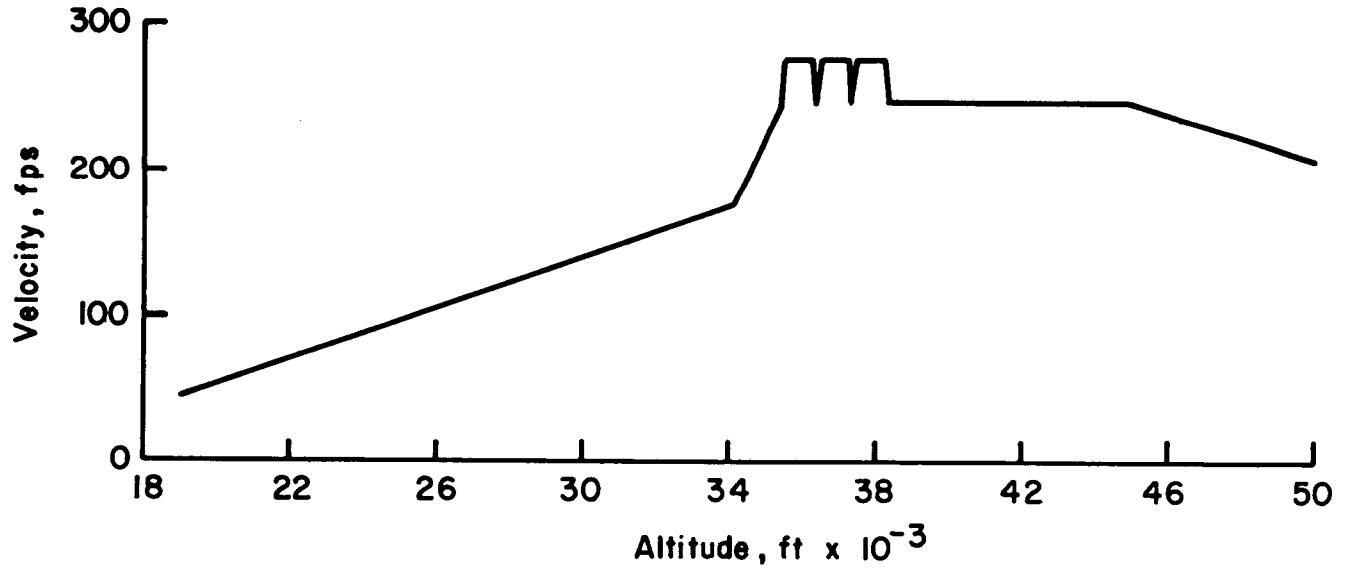

Figure 17 – Saturn V wind input

~~CONFIDENTIAL~~

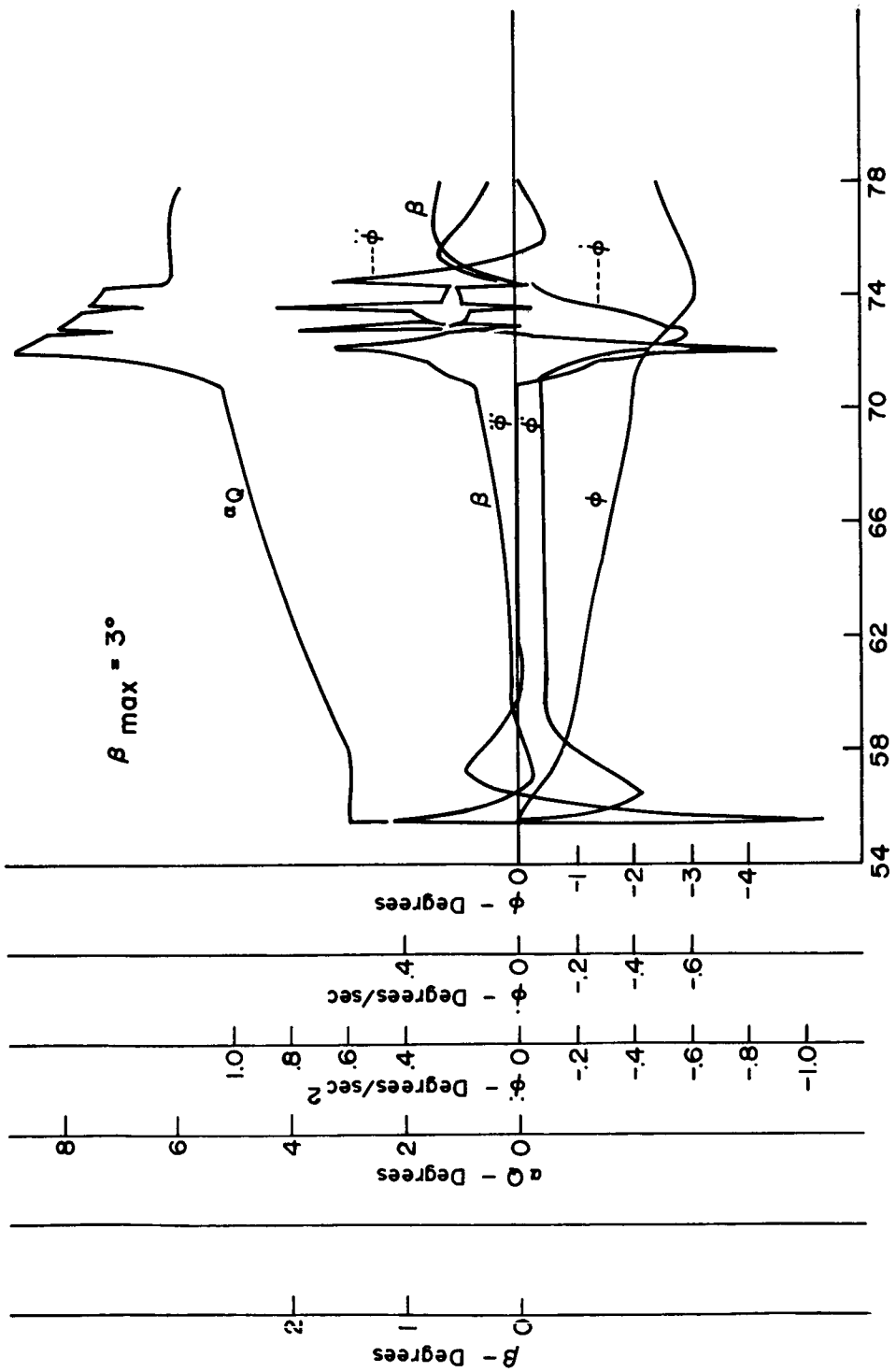

~~CONFIDENTIAL~~

Figure 18 – Saturn IV control response to 95% probability level wind profile

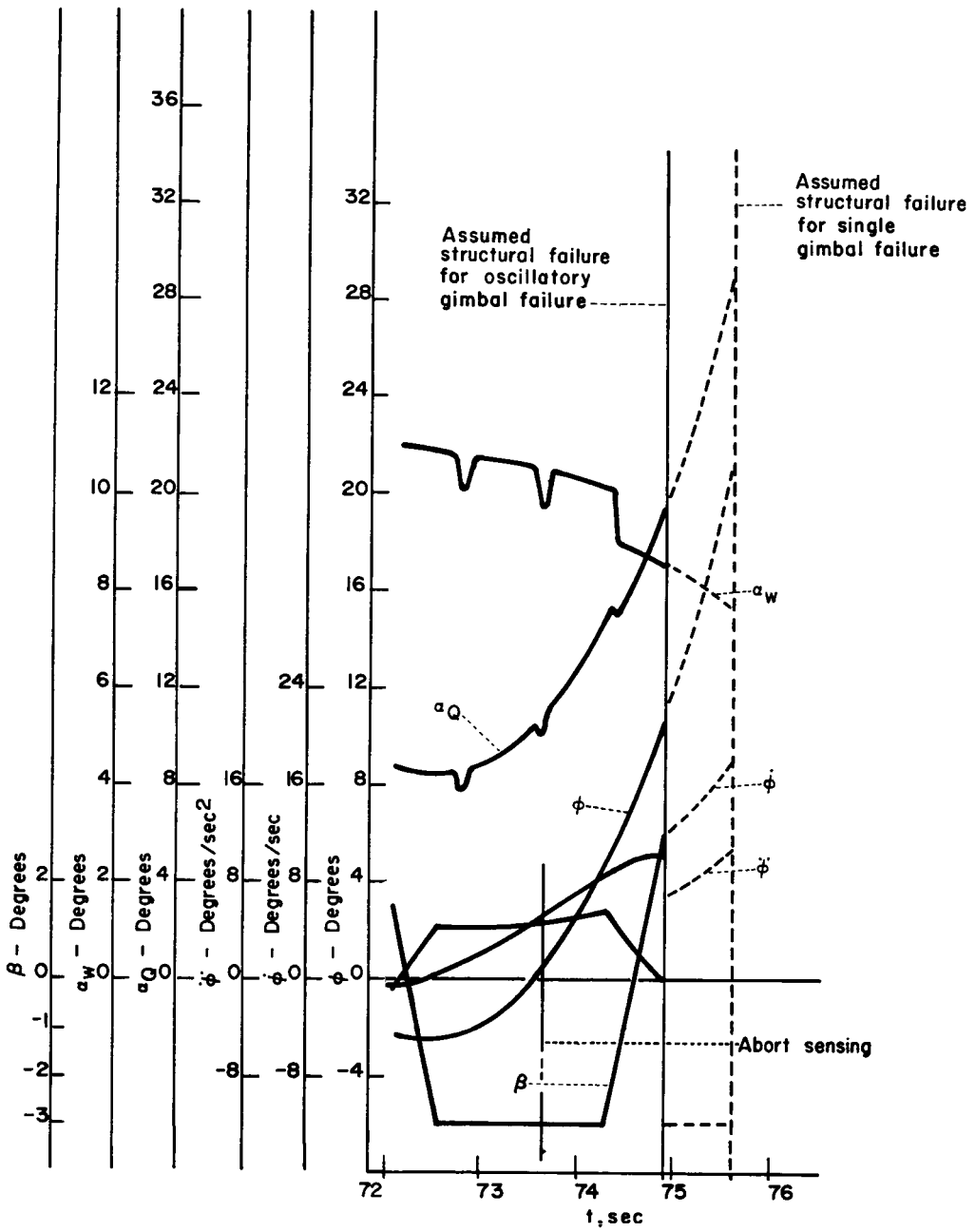

Figure 19 - Saturn V divergence study - control motors hard over at q_{max}

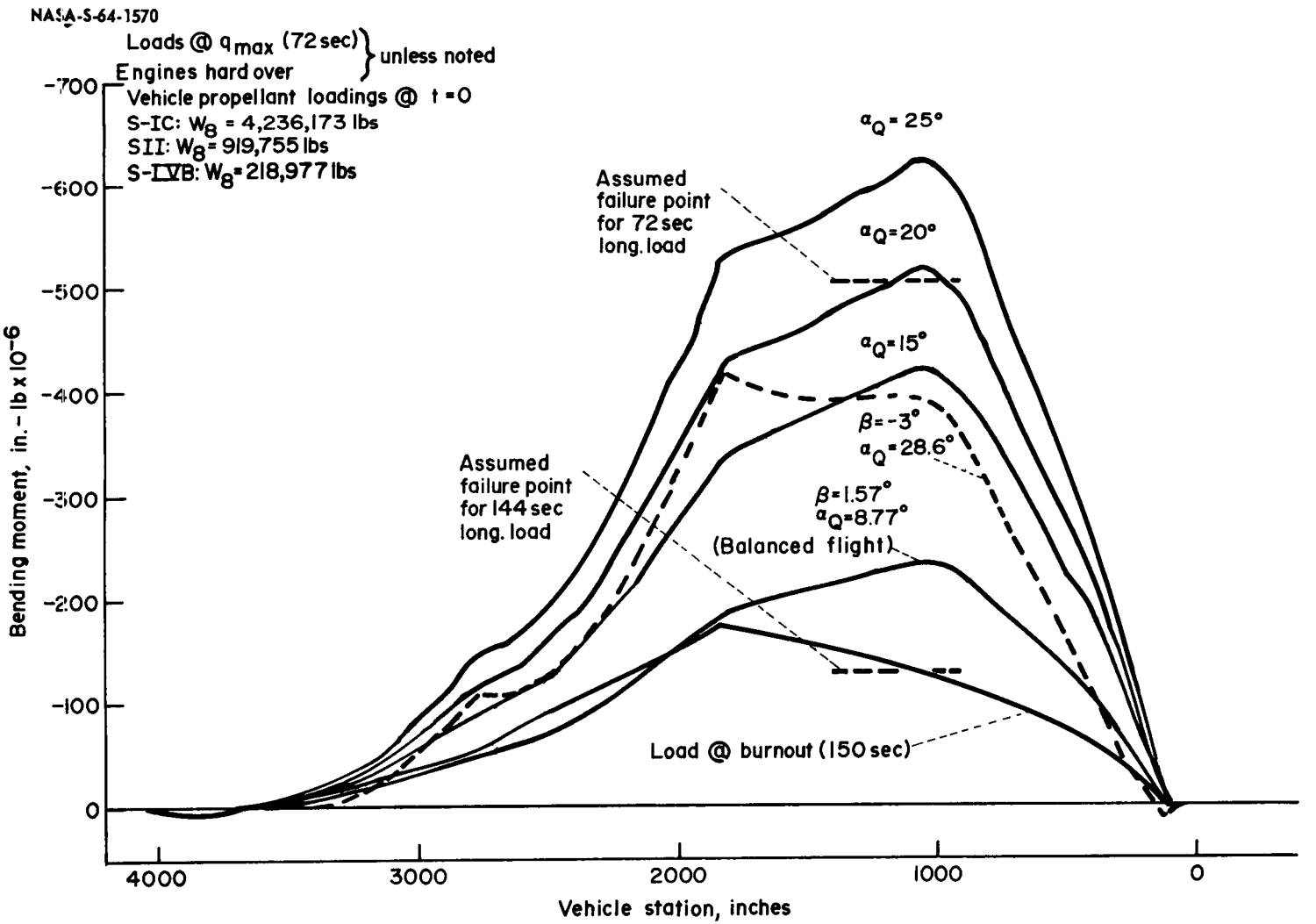

Figure 20- Saturn V expected bending moment distributions

NASA-S-64-1553

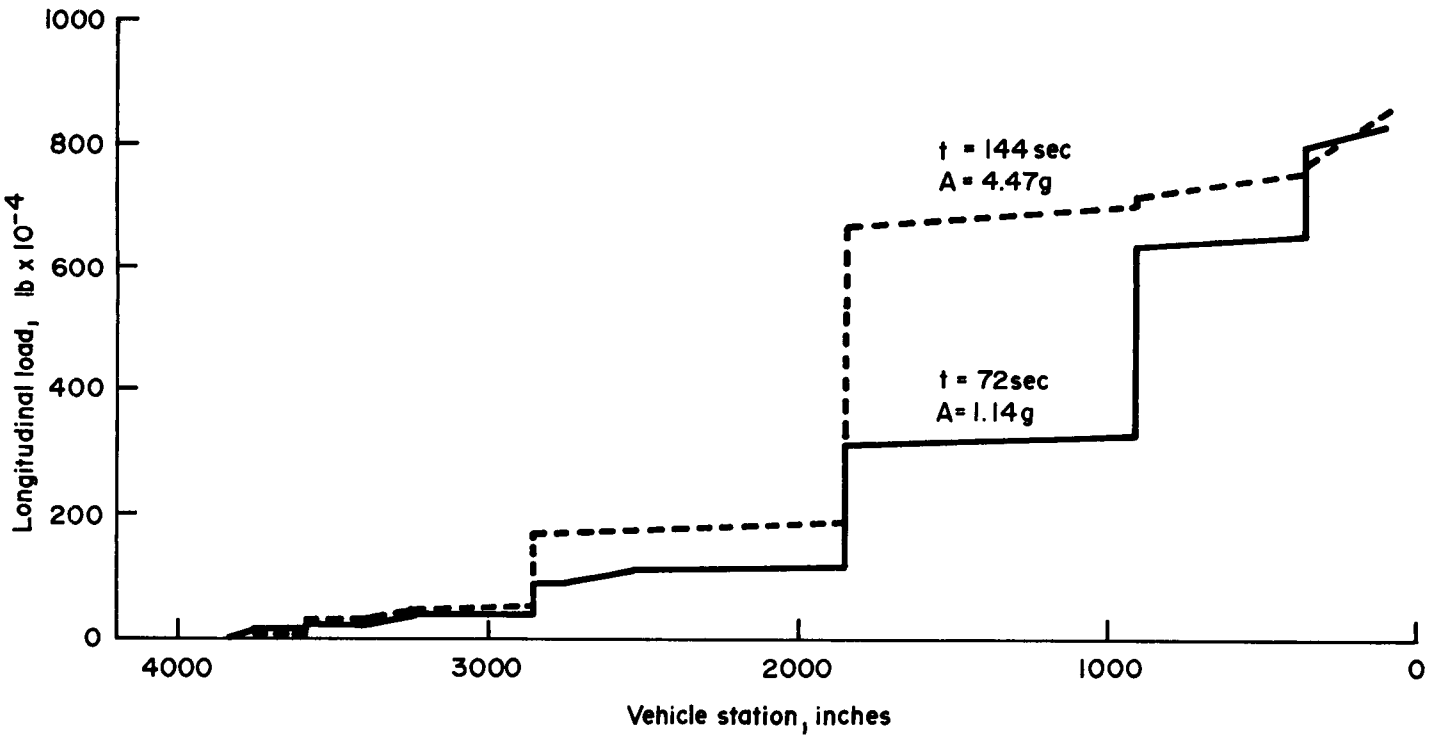

Figure 21 - Saturn V longitudinal load distributions

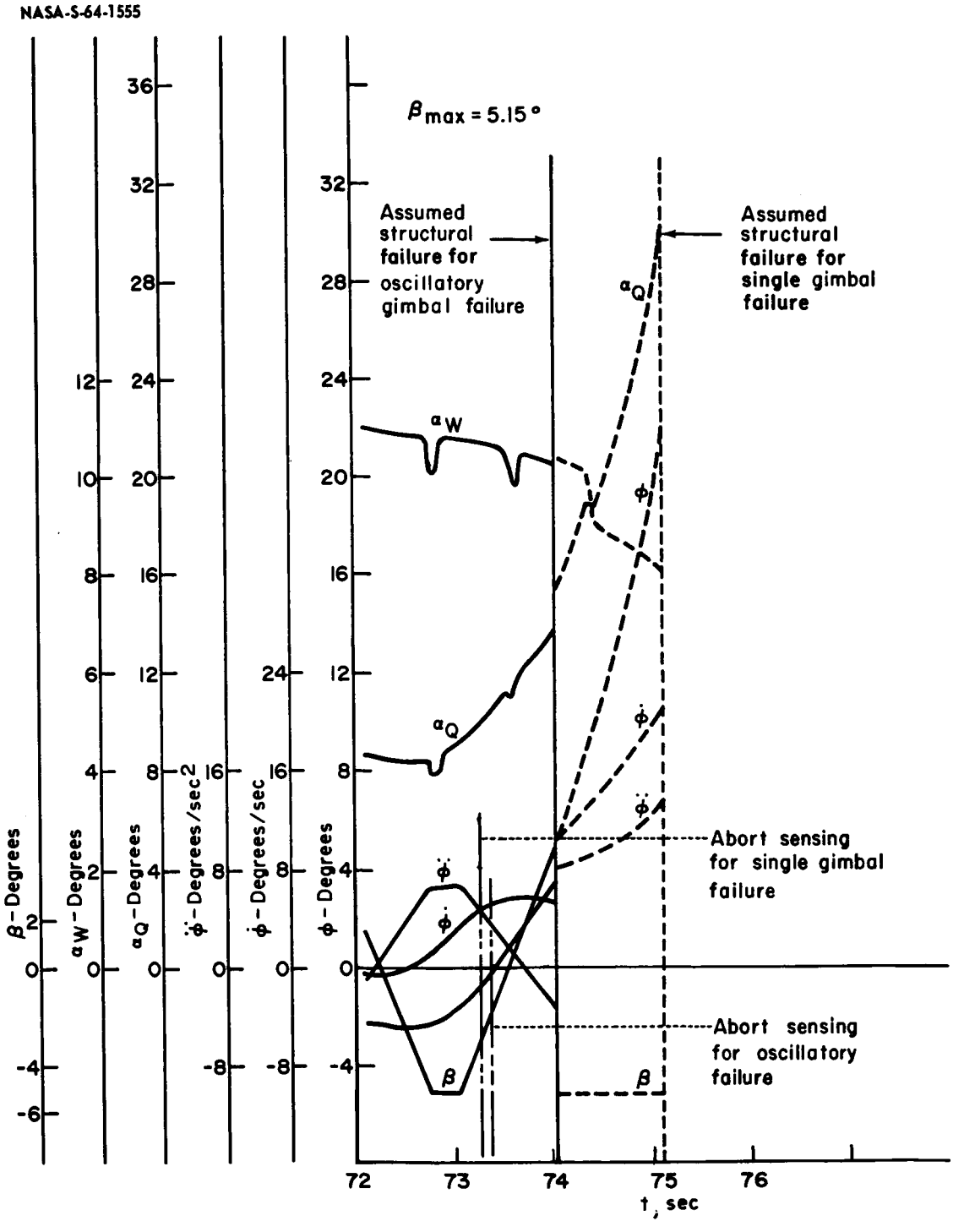

Figure 22-Saturn V divergence study-control motors hard over at q_{max}

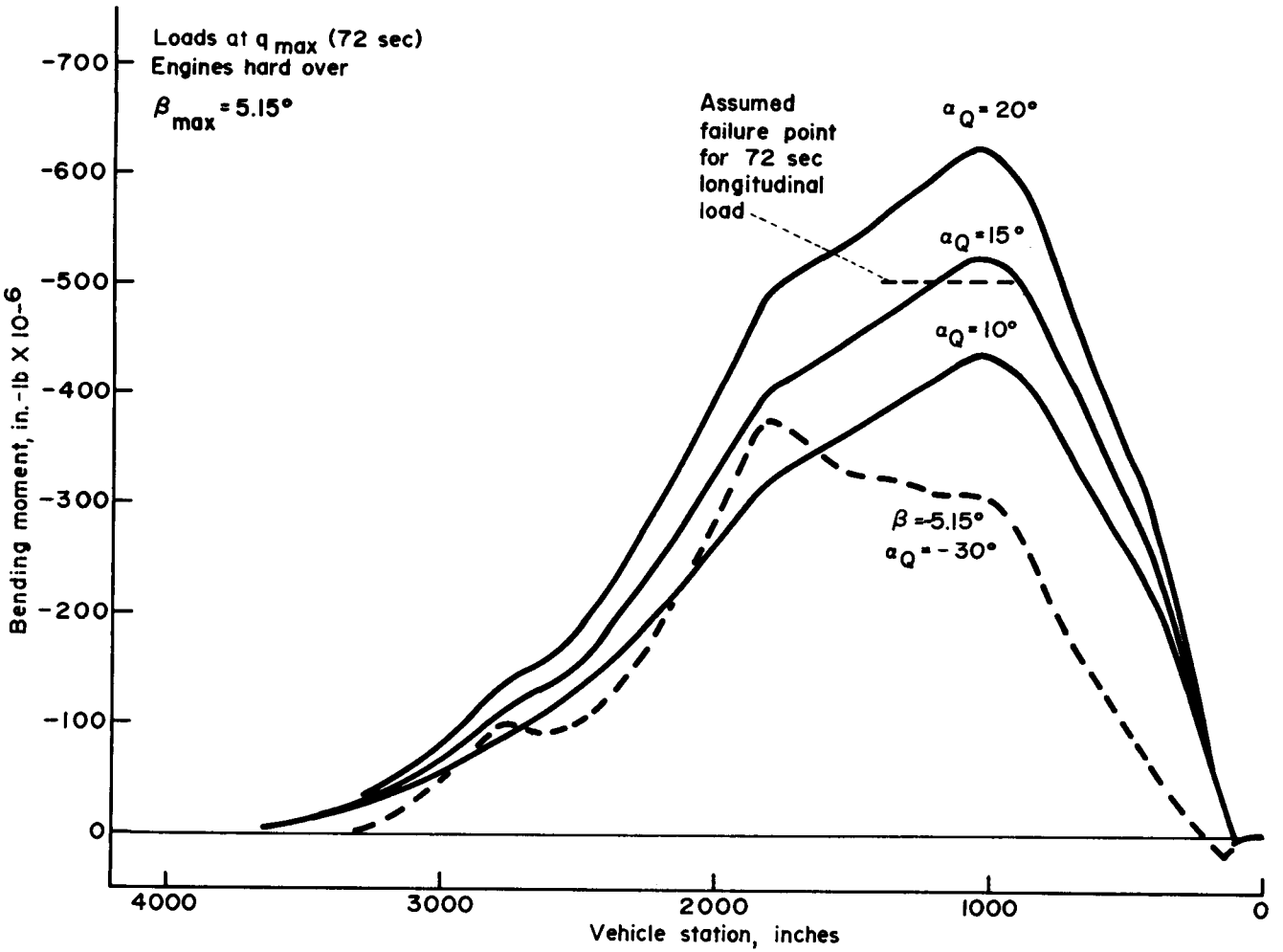

Figure 23 - Saturn V expected bending moment distributions

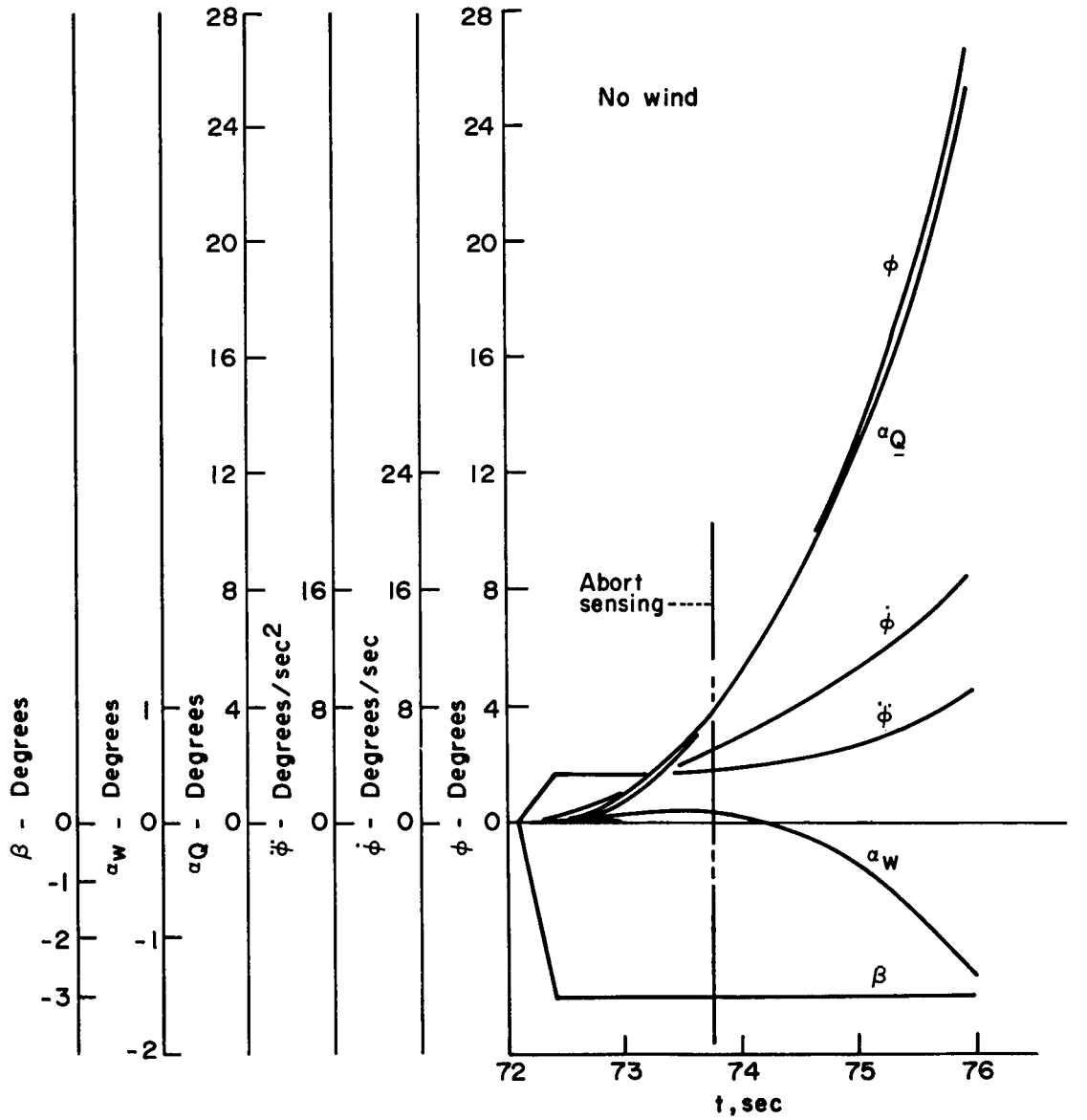

Figure 24-Saturn V divergence study-control motors hard over at q_{max}

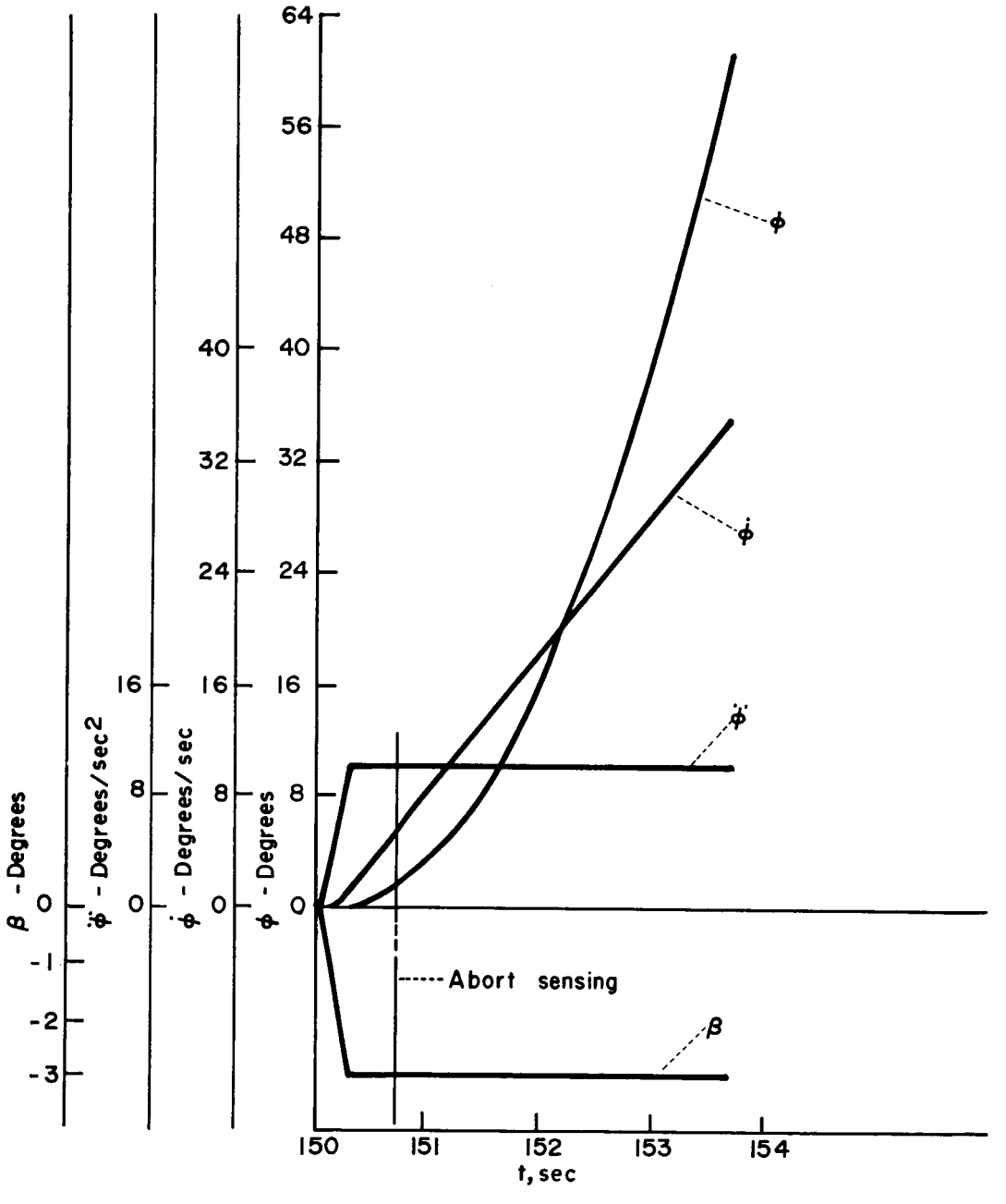

Figure 25-Saturn V divergence study-control motors hard over at burnout

NASA-S-64-1552

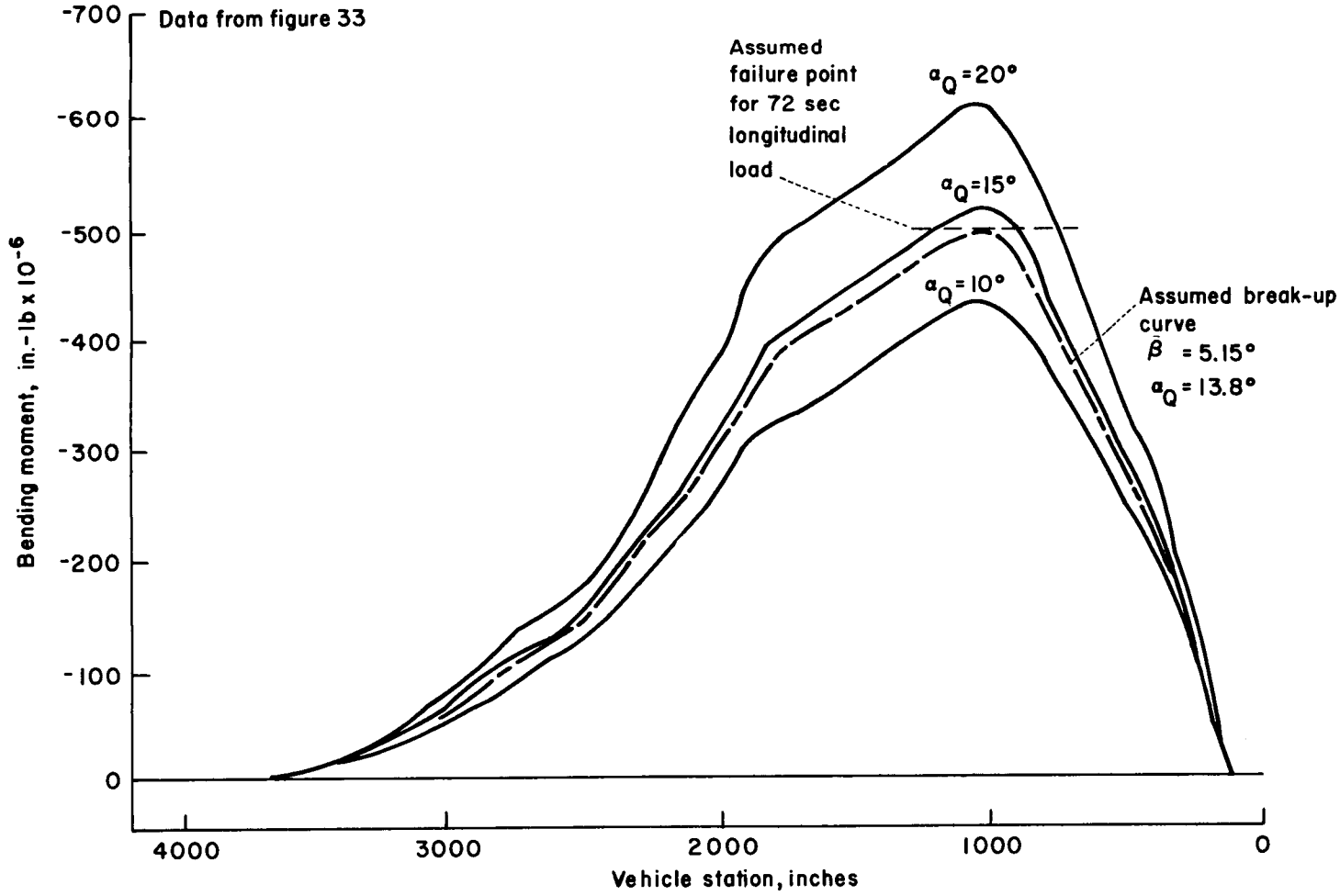

Figure 26- Illustrated example of procedure for determining break-up bending moment curves and angles-of-attack